

## Research Article

# Foraminiferal analysis of Holocene sea-level rise within the Trinity River Incised Paleo-Valley, Offshore Galveston Bay, Texas

P. Standring<sup>a,b,\*</sup>, C.M. Lowery<sup>a</sup>, J. Burstein<sup>a,b,1</sup>, J. Swartz<sup>a,b,2</sup>, J.A. Goff<sup>a</sup>, S.P.S. Gulick<sup>a,b</sup>, C.B. Miller<sup>a,b</sup>

<sup>a</sup> Institute for Geophysics, University of Texas at Austin, Austin, TX, United States of America

<sup>b</sup> Department of Earth and Planetary Sciences, University of Texas at Austin, Austin, TX, United States of America

## ARTICLE INFO

Editor: Edward Anthony

## Keywords:

Sea level change  
Micropaleontology (forams)  
N America

## ABSTRACT

Regional variability of global sea-level rise remains an important area of study given the vulnerability of sediment-starved coastlines to coastal inundation, especially those in proximity to large population centers. Galveston Bay, Texas, is currently experiencing more than double the global rate of sea-level rise and is particularly vulnerable to storm inundation that will further destabilize the coastline. Limitations in instrumental observations necessitate the use of the geologic record preserved offshore modern Galveston Bay to understand how this particular coastline responds to periods of rapid sea-level rise. We present micropaleontological analysis of sediment cores combined with high-resolution seismic data to reconstruct the Holocene paleoestuary offshore Galveston Bay and its evolution since initial inundation ~10 ka through marine transgression ~6 ka. We find that despite rapid sea-level rise, the Galveston paleoestuary maintained relatively stable outer boundaries, and within the bay environmental shifts occurred as a result of probable marine incursions due to tidal inlet migrations. Paleoenvironmental changes in the early Holocene coincide with flooding events within other Texas Gulf Coast bays suggesting global sea-level rise played a prominent role. Middle to late Holocene changes occurred when rates of sea-level rise slowed, suggesting regional hydroclimate change played a more dominant role.

## 1. Introduction

Constraining the regionally variable impact of rising sea level is increasingly important for coastal planning (Vitousek et al., 2017). Regional variability of sea-level rise is particularly evident in Galveston Bay, Texas. Low-gradient, low-elevation coastlines all around the Gulf of Mexico are especially vulnerable to sea-level rise and the destruction caused by large storms and hurricanes (Bernstein et al., 2019; FitzGerald et al., 2008; Goff et al., 2010; Palermo et al., 2021; Shawler et al., 2021). Mean annual sea level rates at Galveston Bay Pier 21 are  $+6.63 \pm 0.21$  mm yr<sup>-1</sup> from 1904 to 2020 (NOAA, 2023). This rate is significantly higher than all other stations along the Texas Coast, and even double in some cases. For example, South Padre Island and Port Mansfield in south Texas are experiencing rates of sea-level rise of  $+4.23 \pm 0.51$  mm yr<sup>-1</sup> and  $+3.69 \pm 0.66$  mm yr<sup>-1</sup>, respectively (NOAA, 2023).

The modern rate of sea-level rise in Galveston Bay exceeds that of the

last 10 kyr, when waning melting of ice sheets slowed global sea-level rise from 4.2 mm yr<sup>-1</sup> to 1.4 mm yr<sup>-1</sup> (Anderson et al., 2022; Milliken et al., 2008). Extensive work by John Anderson and colleagues in several Gulf Coast estuaries revealed several rapid flooding events when the entire estuary and barrier island system retreated landward by several kilometers (Anderson et al., 2022, Anderson et al., 2016, Anderson et al., 2014, Anderson et al., 2008; Anderson and Rodriguez, 2008; Maddox et al., 2008; Milliken et al., 2008; Milliken et al., 2008b; Milliken et al., 2008cc; Rodriguez, 1999; Rodriguez et al., 2008a, Rodriguez et al., 2008b, Rodriguez et al., 2005, Rodriguez et al., 2004, Rodriguez et al., 2001, Rodriguez et al., 1999; Simms et al., 2008; Siringan, 1993; Siringan and Anderson, 1994; Siringan and Anderson, 1993; Thomas and Anderson, 1994). These major events occurred on the order of ~1000 years, and apparently punctuated intervals of relative stability. An estuary can be considered stable while maintaining its external boundaries (i.e., barrier island system) and still undergo environmental change

\* Corresponding author at: Institute for Geophysics, University of Texas at Austin, Austin, TX, United States of America.

E-mail address: [patty.standring@utexas.edu](mailto:patty.standring@utexas.edu) (P. Standring).

<sup>1</sup> Now at: OARS Group – Marine Geoscience Consultants, Houston, Texas

<sup>2</sup> Now at: Water Institute of the Gulf, Baton Rouge, Louisiana

<https://doi.org/10.1016/j.margo.2024.107345>

Received 11 December 2023; Received in revised form 19 June 2024; Accepted 26 June 2024

Available online 4 July 2024

0025-3227/© 2024 Elsevier B.V. All rights reserved, including those for text and data mining, AI training, and similar technologies.

within the estuary (e.g., salinity variability due to increased marine mixing or higher fluvial input). Characterizing those intervals of stability is essential for understanding how the modern Galveston Bay system will respond to renewed sea-level rise. Can change occur during these periods of stability? Is there a sea level threshold that produces estuarine instability in the system? The physics are currently unclear.

Benthic foraminiferal assemblages provide a sensitive indicator of bay environment that can record more gradual changes than those typically reconstructed from mollusks in core samples. Here, we integrate high-resolution seismic data published by Burstein et al. (2023) and Swartz et al. (2022) with micropaleontological analysis, sedimentology, and a radiocarbon-based age model from sediment cores in the paleo-Trinity estuary system offshore of modern Galveston Bay (Fig. 1) to develop a comprehensive history of Holocene paleoenvironmental and coastal change in the Trinity paleo-valley over the last 10 kyr. We identify periods in which barrier island development helped maintain a stable paleoestuary prior to marine transgression.

## 2. Regional setting/Background

Galveston Bay is located on the northeast Texas coast on the Gulf of Mexico and consists of three bays (East, Trinity, and Galveston bays) that comprise the estuary complex (Fig. 1). The microtidal, wave-dominated regime in the Gulf of Mexico allows for long, narrow, relatively straight barrier island system protecting the estuary, consisting of Bolivar Peninsula on the eastern side of the bay and Galveston Island on the western side (Anderson et al., 2016; Anderson et al., 2014; Anderson et al., 2008; Davis and Hayes, 1984; FitzGerald et al., 2008; Rodriguez et al., 2004).

John Anderson and colleagues at Rice University established a firm foundation of research on modern Galveston Bay and its transformation throughout the Holocene (Anderson et al., 2022; Anderson et al., 2016; Anderson et al., 2014; Anderson et al., 2008; Milliken et al., 2008; Rodriguez et al., 2005; Rodriguez et al., 2004; Simms et al., 2008; Siringan and Anderson, 1993; Thomas and Anderson, 1994). During Marine Isotope Stages (MIS) 5–3, the region experienced episodic sea level fall, which led to the creation of Trinity and San Jacinto incised river valley (Fig. 2A & 2C) (Anderson et al., 2016; Anderson et al., 2014; Swartz et al., 2022). Stepped downcutting throughout the incised valley resulted in terraced morphology (Anderson et al., 2016; Anderson et al.,

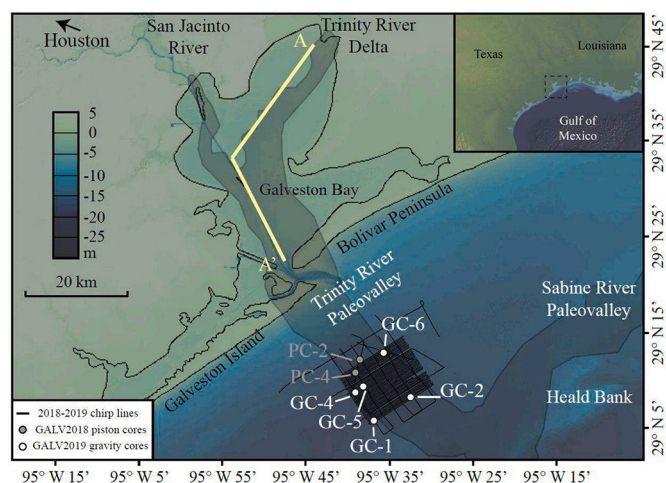


**Fig. 1.** Study area offshore Galveston Bay, Texas, with Trinity River incised valley (gray outline), A-A' profile of cross-section shown in Fig. 4 from Anderson et al. (2008), high-resolution seismic lines (black lines), 2018 piston cores (gray circles), and 2019 gravity cores (white circles). Base map made with GeoMapApp (www.geomapapp.org) and the National Centers for Environmental Information (formerly NGDC) Coastal Relief Model (NOAA NCEI, 2023).

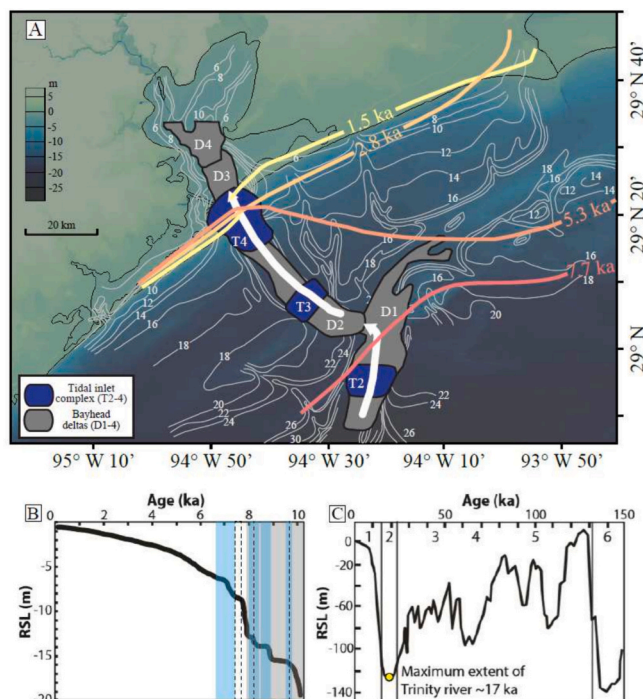


**Fig. 2.** A) Map of modern Galveston Bay with topographic contours of the Holocene-Pleistocene surface (redrawn from Siringan, 1993), backstepping bayhead deltas with associated tidal inlets infilling the Trinity River incised valley during Holocene transgression (modified from Swartz, 2019), and the current paleoshoreline model for Galveston Bay (redrawn from Rodriguez et al., 2004). Base map made with GeoMapApp (www.geomapapp.org) and the National Centers for Environmental Information (formerly NGDC) Coastal Relief Model (NOAA NCEI, 2023). B) Sea level rise over the last 10 kyr showing periods of rapid sea level rise identified by Milliken et al. (2008a) (shaded blue) and rapid sea level rise in Galveston Bay, Texas, identified by Anderson et al. (2008) (dashed lines). C) Holocene sea level curve over last 150 kyr showing Marine Isotope Stages 1–6 and maximum lowstand for the Trinity River occurring approximately 17 ka (modified from Swartz, 2019). (For interpretation of the references to colour in this figure legend, the reader is referred to the web version of this article.)

2008; Rodriguez et al., 2005). The upper, wider portions of the offshore incised valley are not visible in the sediment record because this stratigraphy has been removed by shoreface erosion due to the transgressive ravinement during Holocene sea-level rise. This ravinement occurs at 8 to 10 m depth below the seafloor along the Texas coast, expressed as onlapping marine muds onto a “decapitated shoreface” (Anderson et al., 2016).

Global sea-level rise between ~11.4 and 8.2 ka is estimated at ~15 m kyr<sup>-1</sup> followed by a reduced rate of sea-level rise 8.2–6.7 ka, coinciding with the final deglaciation of North America (Lambeck et al., 2014). Along the Gulf Coast, sea level began to rise episodically between ~10 and 7 ka, after which it slowed to steady present day levels (Fig. 2B) (Anderson et al., 2016; Anderson et al., 2014; Milliken et al., 2008; Swartz, 2019). Multiple proposed flooding surfaces within the Trinity incised valley occur either contemporaneously with other areas along the Gulf coast and are attributed to rapid sea-level rise, or exist locally, suggesting forcing mechanisms such as changing sediment supply and/or antecedent topography (Anderson et al., 2022; Anderson et al., 2016; Rodriguez et al., 2005). Radiocarbon dating in sediment cores from modern Galveston Bay constrain rapid sea-level rise events to 9.6 ka, 8.2 ka, and between 7.7 and 7.4 ka, in which each inundation was complete after only a few centuries (Fig. 2B & 3) (Anderson et al., 2022; Anderson et al., 2008). Milliken et al. (2008a) identified flooding events consistent with radiocarbon dates and relative sea level changes within the Gulf of Mexico at 9.5–9.8 ka, 8.5–8.9 ka, 8.0–8.4 ka, and 6.8–7.4 ka (Fig. 2B).

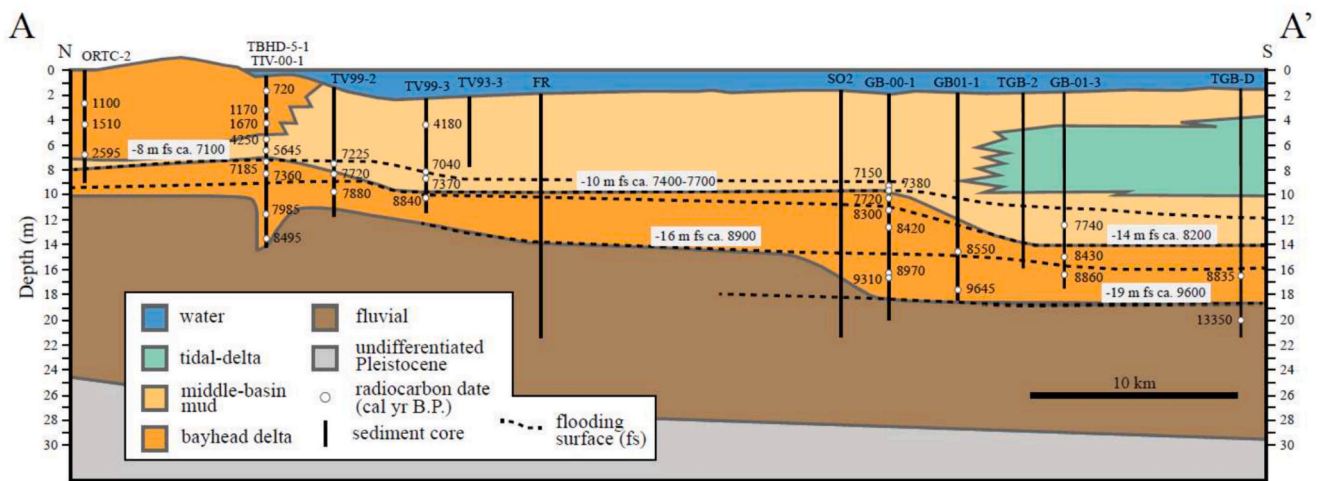


Fig. 3. Cross section of the Trinity River Paleovalley in modern Galveston Bay, Texas (location in Fig. 1), compiled from seismic and core data analyzed by Anderson Group displaying prominent sedimentary facies and flooding surfaces with radiocarbon ages (redrawn from Anderson et al., 2008).

Approximately 9.6 ka, the initial inundation of modern Galveston Bay shifted the upper bay ~30 km up the incised valley, coincident with Laurentide Ice Sheet (LIS) retreat and Hudson Strait freshwater drainage (Anderson et al., 2008; Jennings et al., 2015; Lambeck et al., 2014; Thomas and Anderson, 1994) and is primarily attributed to antecedent topography coinciding with rapid sea-level rise events (Anderson et al., 2022; Rodriguez et al., 2008b; Rodriguez et al., 2005). Approximately 8.2 ka, the bayhead delta shifted ~10 km up the valley, partially attributed to a “dramatic decrease in sedimentation rates” from 4.6 mm yr<sup>-1</sup> to 1.3 mm yr<sup>-1</sup> and the elevation of a Pleistocene-age terrace (Fig. 3, Anderson et al., 2008) but coinciding with LIS melting events at ~8.6 ka and 8.15 ka (Jennings et al., 2015). Between 7.7 and 7.4 ka the upper bay shifted a farther ~25 km up the valley at a rate of 8 km century<sup>-1</sup> but maintained its existing shoreline ~50 km seaward of the modern coastline, which produced a ~100-km-long paleoestuary (Anderson et al., 2008; Rodriguez et al., 2005). This flooding event occurred despite the decreasing rate of sea-level rise between 7.5 and 7.0 ka, with coincident events in Matagorda Bay (Maddox et al., 2008) and Sabine Lake (Milliken et al., 2008c), and is attributed to a Gulf Coast climate transition from cool and moist to warm and dry regimes, reducing sediment supply (Anderson et al., 2008).

Radiocarbon dating of sediments from Heald Bank suggest that the paleoshoreline was in that location by as late as 7.7 ka, while ages obtained from the oldest beach ridges on Galveston Island constrain the seaward progradation of the island to after 5.3 ka (Fig. 2A) (Anderson et al., 2014; Anderson et al., 2008; Rodriguez et al., 2005; Rodriguez et al., 2004). Prior interpretations of Heald Bank suggest the bank may be marine in origin, like Thomas and Shepard Banks, and developed after the shoreline had already shifted up-valley (Thomas and Anderson, 1994). Bolivar Peninsula began to develop as a spit ~2.5 ka and as it prograded westward, the tidal inlet narrowed to a fraction of its original size to form Bolivar Roads tidal inlet allowing flooding along the bay boundaries, establishing the modern shape of Galveston Bay (Anderson et al., 2016; Anderson et al., 2014; Anderson et al., 2008; Rodriguez et al., 2005; Rodriguez et al., 2004).

Although prior sedimentological, radiocarbon, and seismic research offshore Galveston Bay is thorough (Anderson et al., 2022; Anderson et al., 2016; Anderson et al., 2008; Rodriguez, 1999; Rodriguez et al., 2004), additional higher resolution seismic data combined with radiocarbon dating of sediment cores and micropaleontological interpretations of facies changes will better spatially and temporally constrain the large estuarine environment and the transformation of the coastline throughout the Holocene. Foraminifera are powerful proxies for paleoenvironmental and relative sea level change because of their

sensitivity to temperature, salinity, and nutrient availability (Culver, 1988; Culver et al., 1996; Garrett et al., 2023; Gehrels, 2013; Leckie and Olson, 2003; Phleger, 1951; Poag, 2015; Poag, 1981; Williams, 1994; Woo et al., 1997). Modern assemblages represent a specific physical and chemical environment within ecological niches or biozones that can be translated to fossil assemblages in sediment cores to identify paleoenvironmental changes as a result of relative sea level fluctuations forming a link between observational and fossil records (Culver, 1988; Gehrels, 2013; Leckie and Olson, 2003; Phleger, 1965; Phleger, 1960; Poag, 1981). Foraminiferal paleoecological assemblages have been used extensively to reconstruct depositional environmental change (e.g., Buzas-Stephens et al., 2014; Olson and Leckie, 2003; Wellner et al., 2004). Extensive work on the living assemblages of Galveston Bay was carried out by Wantland (1969) and was combined with unpublished data from William Sliter by Poag (1981) to provide detailed maps of foraminiferal predominance facies in the bay. This assemblage work allows us to differentiate upper, middle, and outer (sometimes referred to as lower) bay environments within otherwise unremarkable successions of estuarine mud and separate sandy ebb- and flood-tidal delta deposits from back-barrier, washover fans. Benthic foraminiferal assemblages provide paleoenvironmental context for seismic data and allow for the clarification of the timing of the inundation of the Trinity River Paleovalley and the interpretation of barrier island stability and rollover rate amid rising sea levels at a higher resolution than has previously been possible.

### 3. Methods

#### 3.1. Seismic data

Approximately 700 km of high-resolution seismic data were collected during three cruises in 2017 to 2018. These surveys were conducted with an EdgeTech 512i sub-bottom profiler with 0.7 to 12 kHz frequency sweep and 20-ms pulse length (Fig. 1). Extensive discussion of seismic data processing and interpretation (including images of uninterpreted lines) can be found in Swartz et al. (2022) and Burstein et al. (2023). Seismic lines corresponding to sediment cores were converted from two-way travel time in milliseconds to meters with an approximate seismic wave velocity of 1525 m s<sup>-1</sup> based on average values from Exxon surveys of the Brazos River delta region to the west of our study area (Abdulah et al., 2004).



### 3.2. Piston and gravity coring

Piston core (PC) sites (Fig. 1) were chosen based on sedimentary structures observed in seismic data to pinpoint key transitions in the sedimentary record and evaluate paleoenvironmental evolution from fluvial to estuarine to modern-day marine. The cores were collected on the R/V *Brooks McCall* during the University of Texas Institute for Geophysics 2018 Marine Geology and Geophysics (MG&G) Field Course. Gravity cores (GC) were collected on a subsequent cruise of the R/V *Manta* in 2019 (Fig. 1) and were located to clarify additional seismic horizons of interest, particularly along the valley edges.

Cores were split onshore after both cruises were completed. The archive halves were stored, and the working halves were described for appearance, qualitative grain size, bioturbation, and presence of marine fauna (e.g., shell fragments and shell hash), and terrestrial organic material (e.g., plant debris) and then sampled for quantitative grain size analysis, microfossil analysis, and carbon dating. Microfossil analysis samples (~10 cm<sup>3</sup> of material) were selected at 10- to 50-cm intervals, and at specific points where a paleoenvironmental transition may have occurred based on changes observed in the core, generally avoiding sandier sediments, which tend to contain few (and often reworked) foraminifera. Piston core 2 (PC-2) was the longest core collected and was sampled at higher resolution to serve as a reference section. Subsequent sampling in PC-4 and all the gravity cores (GC-1 through GC-6) was done at a lower resolution with additional samples selected to more precisely identify paleoenvironmental transitions. Samples were soaked for at least 24 h in a mixture of borax and hydrogen peroxide to break down clay floccules, washed over a 63- $\mu$ m sieve, and dried in an oven at low temperatures (~75 °C).

### 3.3. Foraminiferal analysis

Population abundance analysis is more robust than presence/absence of fossil material in identifying depositional environmental change, and more sensitive to subtle changes. Samples were split in a microsplitter to provide a reasonable amount of material and foraminifera were picked using a binocular microscope in a randomized pattern to avoid bias and placed on a slide. Population sizes of at least 100 foraminifera tests were picked where possible (some samples were barren or did not yield 100 individuals) and identified at the genus level. Foraminifera that were not identifiable at the genus level were classified as “benthic spp.” Confidence interval calculations (Appendix A) following the binomial method of Buzas (1990) show that these population sizes are sufficient to track changes in predominance facies (i.e., *Ammonia* vs. *Elphidium*) within the estuary and recent analysis shows that populations of at least 58 individuals in low diversity assemblages are sufficient for statistical purposes (Forcino et al., 2015). Several modern grab samples from Bolivar Roads tidal inlet obtained during the MG&G 2018 Field Course were analyzed and used as a comparison for flood- and ebb-tidal delta sediments in the cores. Grab samples were soaked overnight in a 1% solution of Rose Bengal and water immediately after collection to stain specimens which were living or recently living. Samples were then sieved and dried in an oven at low temperatures (~75 °C). Populations (living and total) of at least 300 individuals were picked and identified at the genus level (see Appendix A).

Foraminiferal predominance facies in the Gulf of Mexico are defined by genus (Culver, 1988; Poag, 1981). Poag (1981) synthesized analysis of modern benthic foraminiferal assemblages in the Gulf (Fig. 4) and outlined predominance facies for Galveston estuary complex based on the previous work conducted by Wantland (1969) within the Trinity Bay and unpublished work from William V. Sliter of the USGS. Wantland (1969) collected 87 samples from stations within the subaerial Trinity

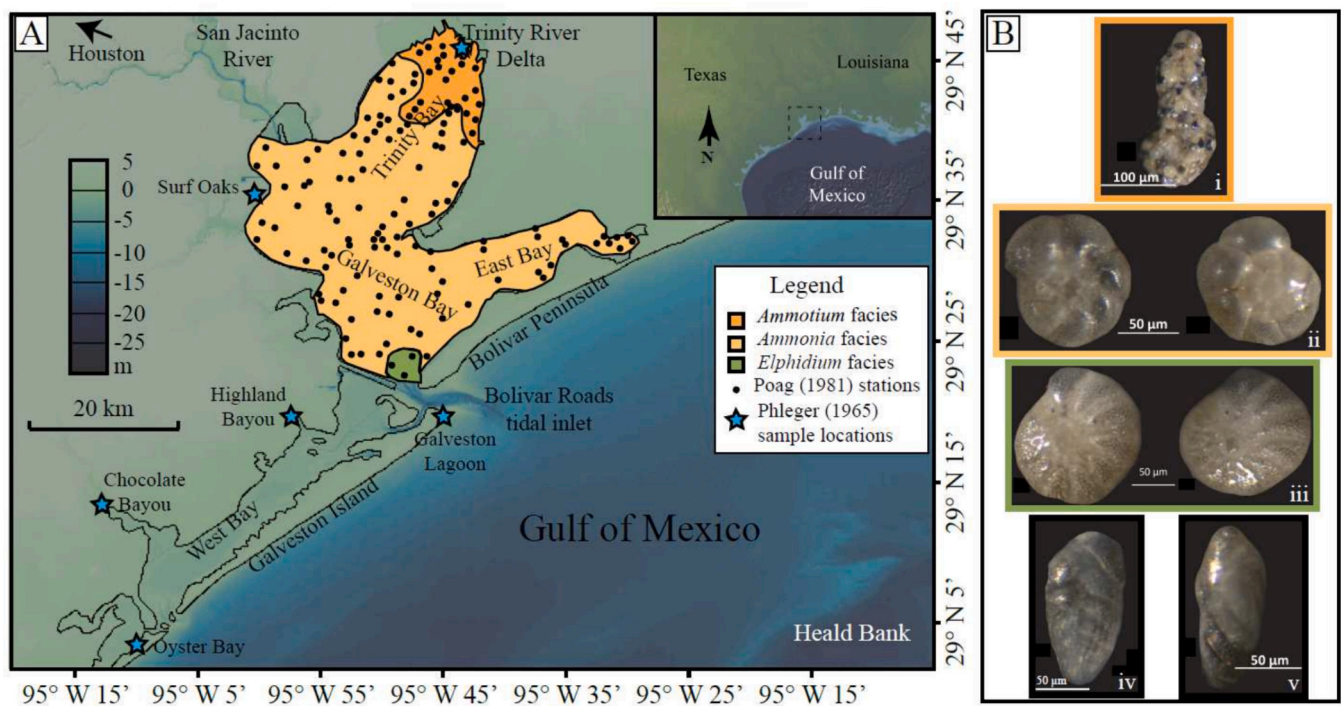


Fig. 4. Foraminiferal predominance facies of Galveston Bay, Texas, based on Poag (1981). A) Map of Galveston Bay, Texas, showing areas within the modern estuary that are dominated by specific genera of foraminifera, and locations of marshes (blue stars) studied by Phleger (1965). B) Images of dominant genera of foraminifera: i) *Ammotium salsum* (orange; upper bay facies), ii) *Ammonia* sp. (yellow-orange; central bay facies), iii) *Elphidium* sp. (green; outer bay facies), iv and v) *Bolivina* sp. and *Bulimina* sp., respectively, which are diagnostic genera for inner shelf facies (Culver, 1988) (modified from Poag, 1981, and Phleger, 1965). Figure made with GeoMapApp ([www.geomapp.org](http://www.geomapp.org)) and the National Centers for Environmental Information (formerly NGDC) Coastal Relief Model (NOAA NCEI, 2023). (For interpretation of the references to colour in this figure legend, the reader is referred to the web version of this article.)



River delta and Trinity Bay and used Rose Bengal solution to determine live taxa at time of collection. Live samples were picked from 62- $\mu$ m sieved wet sediments and populations were based on at least 300 individual tests where possible (Wantland, 1969). Poag (1981) identified the following modern predominance facies for Galveston Bay: dominance of *Ammotium* indicates upper bay or river delta facies (sometimes referred to as bayhead delta), dominance of *Ammonia* indicates central bay facies, and dominance of *Elphidium* indicates outer bay (sometimes referred to as lower bay) facies (Fig. 4). In an effort to match Poag (1981)'s predominance facies, we adopt the terminology of upper bay when describing portions of the estuary that are proximal to the river delta are fresher and outer bay for more saline areas closer to the estuary mouth. Culver (1988) also outlined a priori groups of prominent foraminifera genera by depth and environmental preference, which match well with Poag's predominance facies. Culver (1988)'s diagnostic genera include, *Ammotium* for marshes, *Ammobaculites* and *Elphidium* for bays/estuaries, and *Bolivina*, *Bulimina*, and *Elphidium* for inner shelf environments (Fig. 4).

Paleoenvironmental interpretations of the Holocene estuary system are based off of assemblage percentages of three primary genera outlined by Poag (1981). Samples with >50% *Ammonia* are interpreted as central bay facies, samples with ~50–50% *Ammonia/Elphidium* are transitional to outer bay, and samples with >50% *Elphidium* are outer bay facies. *Ammotium*, indicative of Poag's upper bay (bayhead delta) facies, was very rare and poorly preserved in our cores, as were agglutinated taxa more generally, and so we lumped them all together as agglutinated spp. An overall increase in diversity including common inner shelf taxa (e.g., *Bulimina*, *Bolivina*, miliolids, etc.), typically coupled with a resurgence of *Ammonia* spp., likely indicates a transition to modern marine or open shelf facies (Culver, 1988; Leckie and Olson, 2003; Poag, 1981).

Estuaries are dynamic environments and reworking of material is likely common. To identify areas of potential reworking, foraminiferal test fragments (interpreted to be broken during redeposition) within each sample were counted in addition to individual identifiable tests for population totals. Total fragments were normalized to total foraminifera to provide a percent fragmentation for each sample. Peaks in fragmentation are interpreted as potential periods of increased energy or sediment reworking.

### 3.4. Radiocarbon dating

Sediment cores were sampled for radiocarbon dating to provide age constraints on paleoenvironmental transitions and develop age models for each core. A total of 28 samples were sent to the National Ocean Sciences Accelerator Mass Spectrometry (NOSAMS) at Woods Hole Oceanographic Institute for radiocarbon dating using the Libby half-life of 5568 yr and corrected for carbon isotopic fractionation. Of these samples, 23 were mollusk shells, 2 were comprised of foraminiferal tests, and 3 were plant debris (Table 1). Attempts were made to select articulated mollusk shells for dating, but the absence of these shells precluded their use for radiocarbon dating. Mollusk shell species were not identified because it was deemed unnecessary to use macrofauna as depositional environmental indicators in conjunction with the more precise foraminiferal population analysis.

At NOSAMS, mollusk and foraminiferal samples containing at least 4 mg of material underwent hydrolysis where carbon in the samples were converted to CO<sub>2</sub> using a strong acid H<sub>2</sub>PO<sub>3</sub>. Mollusk samples were powdered to allow staff to subsample material >9 mg. Radiocarbon dates from plant material were calibrated with IntCal20 (Reimer et al., 2020) and mollusk and foraminifera ages were corrected for reservoir variations using a correction specific to the Gulf of Mexico offshore Galveston Bay (Wagner et al., 2009) and then calibrated using Marine20 (Heaton et al., 2020). The IntCal20 calibrations were done via the online program OxCal 4.4 (Ramsey, 2009) and the Marine20 calibrations were applied through the R package Bchron (Haslett and Parnell, 2008). Errors in ages were calculated by NOSAMS where the error is determined

**Table 1**

List of radiocarbon dating samples and their calibrated ages.

No.	NOSAMS OS No.	Sample	Type	Process	Calibrated Age	
					Age (yr)	Error ( $\pm$ yr)
1	155814	PC-2-S3-7-8.5	Mollusk	Hydrolysis	7441	127
2	152146	PC-2-S3-82-83.5	Mollusk	Hydrolysis	7800	134
3	152138	PC-2-S2-69.5-71	Mollusk	Hydrolysis	8468	135
4	152145	PC-2-S2-100.5-102	Mollusk	Hydrolysis	8815	175
5	155815	PC-2-S1-14-16	Mollusk	Hydrolysis	9380	133
6	155816	PC-2-S1-23-25	Mollusk	Hydrolysis	9420	124
7	155817	PC-2-S1-102-104	Mollusk	Hydrolysis	9794	215
8	155818	PC-4-S3-58.5-60	Mollusk	Hydrolysis	7787	136
9	152148	PC-4-S3-59	Mollusk	Hydrolysis	41,030	1703
10	155819	PC-4-S2-15-16.5	Mollusk	Hydrolysis	8815	175
11	152147	PC-4-S2-94-96	Mollusk	Hydrolysis	9131	158
12	155820	GC-1-S1-4-6	Foraminifera ( <i>Ammonia</i> , <i>Elphidium</i> , <i>Bolivina</i> , and <i>Bulimina</i> )	Hydrolysis	1753	143
13	152314	GC-1-S1-5-6	Mollusk	Hydrolysis	589	97
14	152315	GC-1-S1-28.5-30	( <i>Ammonia</i> and <i>Elphidium</i> )	Hydrolysis	38,081	1833
15	155821	GC-2-S1-A-59-61	Mollusk	Hydrolysis	6973	170
16	152310	GC-2-S2-144-145	Mollusk	Hydrolysis	8445	135
17	152316	GC-2-S3-6-10	Mollusk	Hydrolysis	8546	173
18	155902	GC-4-S1-55.5-56.5	plant fragments	Combustion	7913	255
19	152149	GC-4-S2-13-13.5	plant fragments	Combustion	7977	221
20	155903	GC-4-S3-120-122	plant fragments	Combustion	8470	144
21	155822	GC-5-S2-3-5	Mollusk	Hydrolysis	6661	169

(continued on next page)

Table 1 (continued)

No.	NOSAMS OS No.	Sample	Type	Process	Calibrated Age	
					Age (yr)	Error ( $\pm$ yr)
22	155823	GC-5-S3-32-37.5	Mollusk	Hydrolysis	8445	135
23	155824	GC-5-S3-74-76	Mollusk	Hydrolysis	8467	130
24	155825	GC-6-S1-11-14	Mollusk	Hydrolysis	>Modern	
25	155826	GC-6-S1-64.5-66	Mollusk	Hydrolysis	4329	165
26	157505	GC-6-S1-111.5-113	Mollusk	Hydrolysis	7760	142
27	157506	GC-6-S1-130-131.5	Mollusk	Hydrolysis	7709	147
28	157511	GC-6-S2-71-72.5	Mollusk	Hydrolysis	8367	181

by the larger of two estimates, the internal statistical error calculated using the total number of  $^{14}\text{C}$  counts (error =  $1/\sqrt{n}$ ) and the external error determined by the ratio of  $^{14}\text{C}$  and  $^{12}\text{C}$  of a sample calculated 10 separate times while the sample was being run.

### 3.5. Age models

Age models were developed using the R code rbacon (Blaauw and Christen, 2011), which calculates sediment accumulation rates based on a gamma autoregressive semiparametric model using a Markov chain Monte Carlo algorithm. The model provides a predictive window with 95% confidence of the age of sediments given depth and radiocarbon age constraints and the assumption of consistent deposition unless hiatuses are applied. Although we suspect a significant amount of erosion may have occurred during transgression, the lack of upper core (modern marine inner shelf) carbon dates limits the application of hiatus depths in the model and extrapolated ages for the upper core are likely incorrect. Interpolated ages from the models for each core (except for GC-1) were used to date environmental transitions between radiocarbon ages, and in a few instances, extrapolated ages were used to identify transitions outside the range of carbon dates.

### 3.6. Grain size analysis

Sediment samples were taken from PC-2, PC-4, GC-5, and GC-6 at 5–30 cm intervals that varied by core depending on qualitative sedimentology. Samples were dried and then soaked in deionized water for 24 h prior to analysis. Samples were then ultrasonified and stirred before transfer to the Malvern Mastersizer 3000 laser grain size analyzer via pipette until obscuration levels reached the required optimum level for analysis. Quantitative grain sizes between 1 and 1000  $\mu\text{m}$  were then used to determine percent abundance of clay, silt, and sand size fractions.

## 4. Results

Sediment cores range from <1 m to ~6.3 m in depth and primarily contain medium-gray mud predominantly composed of clayey-silt with sandy intervals that occasionally coincide with shell hash layers or abundant shell fragments. GC-4 contains more organic material and less

shell material than all the other cores. GC-1 and PC-4 contain sharp and gradual contacts, respectively, between stiff, light-gray Pleistocene clay terraces and Holocene sediments. PC-2 and PC-4 did not contain any analyzable upper seafloor sediments due to coring disturbance. In both cores, the upper core section (0–1 m in PC-4 and 0–1.8 m in PC-2) contains watery mud which sloshed around inside the core liner as the core was brought on deck and laid down to be extruded. These uppermost sections were not split and are included on the stratigraphic columns for these cores as fine mud, with symbols to indicate coring disturbance. Here, we summarize the key observations for each core, proceeding from the most proximal to most distal core.

### 4.1. Piston core (PC) 2

PC-2 was selected for identification of a fluvial terrace toward the western edge of the incised valley (Fig. 5A). It consists primarily of massive medium-gray clayey-silt with sporadic sandy intervals of varying thickness (2–10 cm) that coincide with increased shell fragments and in some cases shell hash layers (Fig. 5). The core catcher contains silty medium sand (Fig. 5). As the reference section representing the complete transition from fluvial to outer bay deposition, this core was sampled at the highest resolution at least every 10 cm (black stars, Fig. 5B) and, thus, contains more variability in foraminiferal abundance analysis due to salinity variability within the paleoestuary through time. Foraminiferal facies changes in PC-2 do not exactly line up with seismic horizons interpreted by Burstein et al. (2023) (Fig. 5), possibly due to the higher sensitivity of foraminifera to environmental change than is visible in geophysical data.

PC-2 is barren of foraminifera from 6.25 to 5.9 m, and we interpret these sandy deposits as fluvial. Barren sediments are overlain by an interval dominated by agglutinated foraminifera (5.9–5.5 m). A mollusk shell at 5.75 m has an age of  $9794 \pm 215$  cal yr B.P. (Fig. 5). By interpolating the sedimentation rate above this sample, we date the top of this unit to ~9.6 ka. From 5.5 to 2.75 m, the core is characterized by a predominance of *Ammonia*, indicating a central bay environment. It is interesting to note that this interval is not uniformly dominated by *Ammonia*, but rather there are also brief increases in *Elphidium*, which may correspond to shifts in salinity caused by migrating position of the inlet or by centennial-scale changes in Trinity River discharge (see Discussion section). Interpolated ages from the age model of this core (Fig. 7B) indicates that this central estuary assemblage existed from at least 9.6 to 8.0 ka, indicating a long period of stability in the estuary system during this time. A mollusk shell at 2.48 m within sediments dominated by *Elphidium* has an age of  $7800 \pm 134$  cal yr B.P., indicating the environment had transitioned to outer bay by ~8.0–7.8 ka. The uppermost ~1.7 m of the core was not analyzed due to coring disturbance.

### 4.2. Piston core 4

PC-4 and subsequent cores were sampled at a lower resolution (black stars, Fig. 6B) than PC-2 (Fig. 5B), therefore the foraminiferal assemblage changes within these cores appear more gradual compared to PC-2. PC-4 was obtained at the location of another fluvial terrace originally interpreted seismically to be a point bar based on seismic data (Fig. 6), but which was instead revealed to be a Pleistocene flood plain deposit comprised of light-gray, stiff Beaumont Clay, into which the MIS5-MIS3 river valley was incised. The terrace is heavily laminated with oxidized sand layers from subaerial exposure (Fig. 6), diagnostic for Pleistocene sediments along the Gulf Coast (Milliken et al., 2008), and contains a calcareous nodule, which are relatively common in the Beaumont Clay (Rehkemper, 1969). The terrace gradually transitions upward into heavily burrowed sand at ~4.4 m depth, and both the terrace and the overlying sandy section (3.7–5.5 m depth) are barren of microfossils and interpreted as fluvial/terrestrial sediments (Fig. 6). At approximately 3.5 m depth, foraminiferal assemblages appear in the sandy sediments

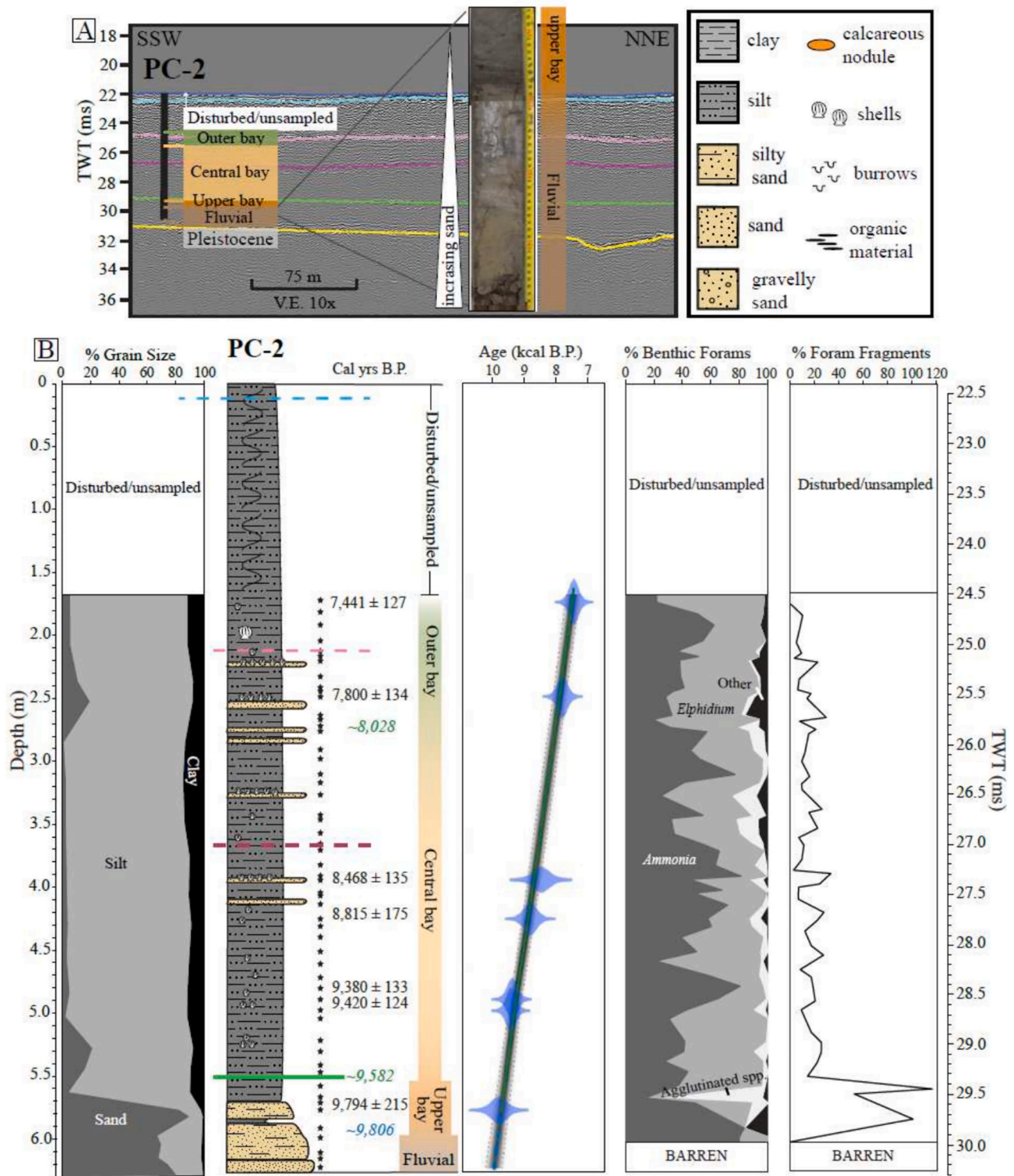


**Fig. 5.** Piston Core 2 (PC-2). A) Interpreted seismic data with approximate depth of penetration for PC-2 (location in Fig. 1). Seismic interpretation from Burstein et al. (2023) (VE = vertical exaggeration) with core image of fluvial to upper bay transition. Seismic interpretation is depicted separately from foraminiferal facies transitions because it does not line up exactly in this core. B) Grain size abundance and stratigraphic column of PC-2 displaying sample locations (black stars), carbon dates (black text), and interpolated (italicized green text) and extrapolated (italicized blue text) ages from age model. Age model based off of radiocarbon ages (blue ovals tapering to error range), with mean age depicted by solid dark green line for interpolated ages, light blue dashed line for extrapolated ages, and gray scale out to 95% confidence interval predicted by the model. Interpreted depositional facies based off of foraminiferal assemblage abundances and percent foram fragments. Two-way travel time scale for stratigraphic column in ms calculated from approximate seismic velocity of 1525 m/s starting at time of seafloor. (For interpretation of the references to colour in this figure legend, the reader is referred to the web version of this article.)



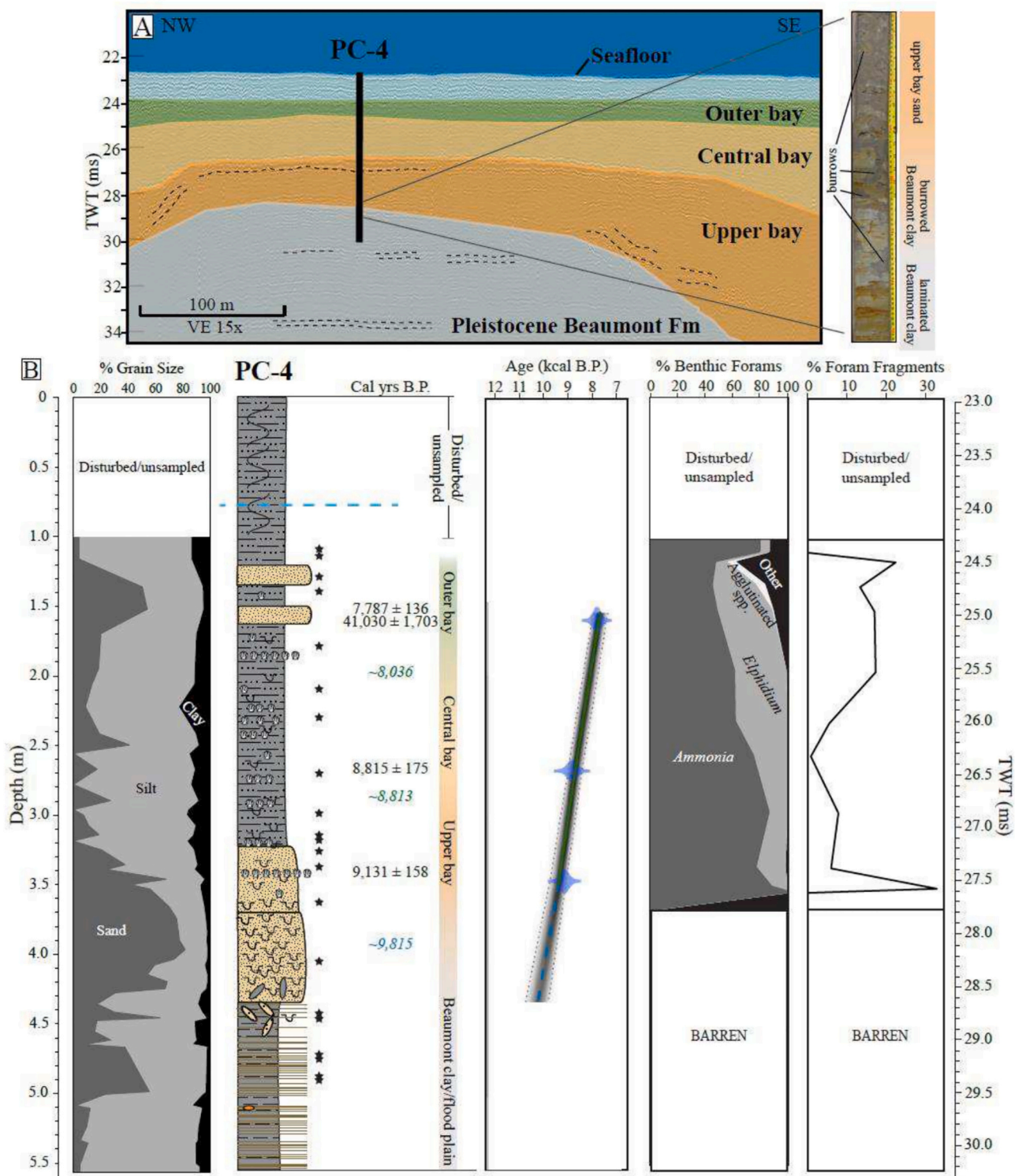


**Fig. 6.** Piston Core 4 (PC-4). A) Interpreted seismic data with approximated depth for PC-4 into a Pleistocene terrace (location in Fig. 1) overlain by paleoenvironment based on micropaleontologic data. Seismic interpretation from Burstein et al. (2023) (VE = vertical exaggeration) with core image showing transition from Pleistocene clay to upper bay sediments. B) Grain size abundance and stratigraphic column with sample locations (black stars), carbon dates (black text), and interpolated (italicized green text) and extrapolated (blue text) ages from age model. Age model based off of radiocarbon ages (blue ovals tapering to error range), with mean age depicted by dark green solid line for interpolated ages, light blue dashed line for extrapolated ages, and gray scale out to 95% confidence interval predicted by the model. Interpreted depositional facies based off of foraminiferal assemblage abundances and percent forams fragments. Two-way travel time scale for stratigraphic column in ms calculated from approximate seismic velocity of 1525 m/s starting at time of seafloor. (For interpretation of the references to colour in this figure legend, the reader is referred to the web version of this article.)

and indicate a transition to an upper bay environment. These sediments contain a mollusk shell at 3.44 m depth with an age of  $9131 \pm 158$  cal yr B.P. and visible burrows with a higher percentage of fragmented foraminifera tests. An extrapolated age from the age model suggests the transition to upper bay took place at  $\sim 9.8$  ka. Central bay sediments ( $\sim 2.0$ – $2.9$  m depth) are dominated by *Ammonia* and contained a mollusk shell at 2.66 m depth dated to  $8815 \pm 175$  cal yr B.P. PC-4 contains less central bay sediments ( $\sim 0.9$  m thick) compared to PC-2 ( $\sim 2.75$  m thick), likely due to the elevation of the Pleistocene terrace. The seismic data show draping of sediments above and over the terrace (Fig. 6A). At approximately 2 m depth, *Elphidium* becomes more dominant and the environment transitions to outer bay sediments. According to the age model for this core (Fig. 6B), the central bay to outer bay transition occurred  $\sim 8.0$  ka, coinciding with the same transition in PC-2. While fragmentation of tests appears low throughout the core, there is a slight increase in the number of fragments in the outer bay section of the core (1.1– $2.0$  m depth), indicating a higher energy environment. The

increase in diversity of foraminifera at  $\sim 1.30$  m depth (e.g., increase in common inner shelf genera, like *Bulimina* and *Bolivina*, and some agglutinated taxa) indicates the beginning of a transition to open marine/inner shelf sediments. This section contains two carbon dates at approximately the same depth (1.59 m) from mollusk shells, one of which likely contains reworked material because it records an unreasonable age for sediments filling a Holocene estuary ( $41,030 \pm 1703$  cal yrs B.P.). The other shell has an age of  $7787 \pm 136$  cal yr B.P. for these outer bay sediments. The upper 1 m section of PC-4 also consisted of soft, disturbed material not suitable for sampling.

### 4.3. Gravity core (GC) 6

Along the eastern edge of the paleovalley, GC-6 penetrated bright seismic reflectors that are represented in the core as a  $\sim 0.8$  m thick sandy package of sediments atop medium-gray estuarine sediments (Fig. 7). Starting at the base of GC-6, clay-sized sediments are dominated

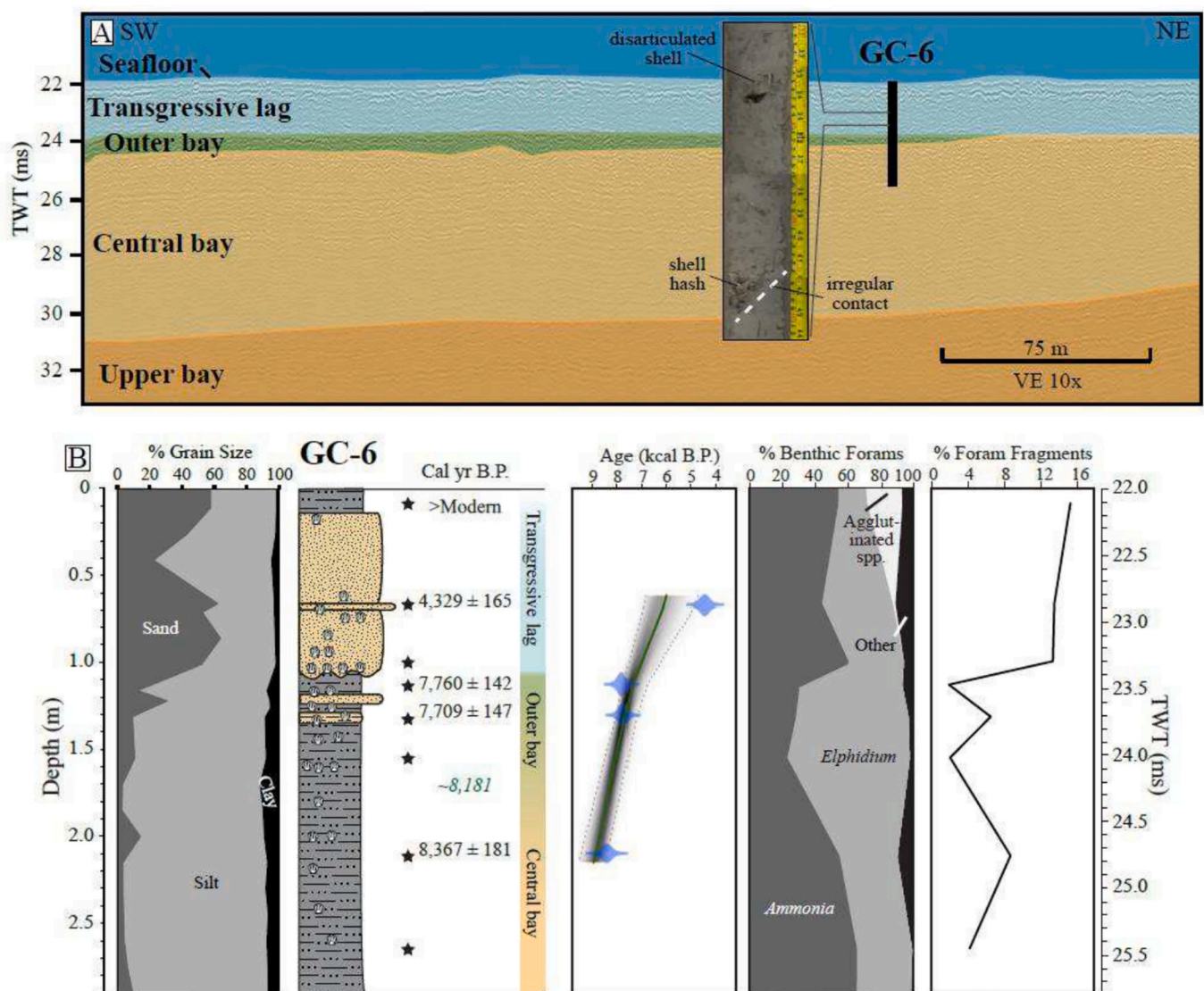


**Fig. 7.** Gravity Core 6 (GC-6). A) Interpreted seismic data with approximate depth of penetration for GC-6 (location in Fig. 1), overlain by paleoenvironment based on micropaleontologic data, and core image of transgressive lag deposit. Seismic interpretation from Burstein et al., 2023 (VE = vertical exaggeration). B) Grain size abundance and stratigraphic column with sample locations (black stars), radiocarbon dates (black text), and interpolated ages (italicized green text) based off of age model. Age model based off of radiocarbon ages (blue ovals tapering to error range), with mean age depicted by solid green line and gray scale out to 95% confidence interval predicted by the model. Interpreted depositional facies based off of foraminiferal assemblage abundances and percent foram fragments. Two-way travel time scale for stratigraphic column in ms calculated from approximate seismic velocity of 1525 m/s starting at time of seafloor. (For interpretation of the references to colour in this figure legend, the reader is referred to the web version of this article.)



by *Ammonia*, indicating a central bay environment; a mollusk shell at ~2.1 m depth indicates an age of  $8367 \pm 181$  Cal yrs. B.P. An increase in *Elphidium* at ~1.7 m depth, with an approximate interpolated age of 8.2 ka based on the age model, indicates a transition to outer bay environment (Fig. 7B). Smaller sandy intervals at the top of the outer bay sediments provide mollusk carbon dates of  $7709 \pm 147$  Cal yr B.P. (~1.3 m depth) and  $7760 \pm 142$  Cal yr B.P. (~1.1 m depth) preceding an irregular contact with the sandy package of sediments (Fig. 7B). Shell fragments decrease in abundance going up the core, while foraminifer test fragmentation increases going up the core, suggesting that the sandy package contains reworked material. A mollusk shell within the sandy package has an age of  $4319 \pm 165$  Cal yrs B.P. Foraminiferal populations suggest a transition from outer bay to inner shelf (increase in inner shelf taxa) was occurring starting at ~1.1 m depth, with the exception of the uppermost sample (GC-6 7–8.5). This uppermost sample contained a foram assemblage that did not match any other assemblages in the study area cores, so it was compared to modern foraminifera assemblages obtained by Phleger (1965) from Galveston Lagoon on Galveston Island, Surfs Oak on the western edge of Galveston Bay, the Trinity River delta, and two grab samples taken from within the flood- and ebb-tidal areas of Bolivar Roads tidal inlet by the MGG 2018 Field Course (Fig. 8, Appendix A). A similar method of foram assemblage comparison was used by Hawkes and Horton (2012) to identify inner shelf-sourced washover sediments from Hurricane Ike on Galveston and San Luis Islands. Our GC-6 comparison revealed that the uppermost sample most closely resembles Phleger's Station 11 sample from Galveston Lagoon (Fig. 8). The lack of extensive plant debris indicates that this is not an in situ back-barrier marsh environment. Rather, we interpret this sandy package as transgressive lag containing reworked barrier island marsh sediments.

#### 4.4. Gravity cores 4 and 5

GC-4 and GC-5 are ~1500 m apart and sample two different seismic facies along parallel seismic lines separated by 1000–1200 m. Both cores contain central bay sediments, with GC-4 close to the lateral margin of the bay and GC-5 closer to the middle. (Figs. 9 & 10). GC-4 penetrates seismic facies along the margin of the incised valley which may explain why it contains the lowest populations of foraminifera of all the cores (all samples are <100 individuals), recording intervals of bay margin sediments barren of foraminifera within central bay and outer bay environments (Fig. 9B). GC-4 primarily consists of medium-gray clayey-silt with a relatively higher amount of organic material, lower amount of shell fragments, lower foraminiferal test fragmentation compared to other cores (the peak in fragmentation is likely an artifact of lower foram population), and more visible burrowing (Fig. 9B). The base of the core contains a barren section (~2.85–3.65 m depth), which is interpreted as bay margin deposits. Plant fragments obtained from 3.35 m depth within these barren sediments were dated to  $8470 \pm 144$  Cal yr B.P. These deposits transition to central bay sediments at ~2.2 m depth, where they are dominated by *Ammonia* and *Elphidium*, and contain less organic material and more burrowing and shell fragments (Fig. 9B). An interpolated age from the age model for this core indicates the transition took place ~8.3 ka. At 1.2 m depth, sediments are again barren of foraminifera and characterized by burrows. Plant fragments from 0.82 m depth have an age of  $7977 \pm 221$  Cal yr B.P. and the age model interpolates the transition to bay margin at ~1.4 m depth to ~8.1 ka. The upper section of the core contains a thin sand interval with plant debris at 0.56 m dated to  $7913 \pm 255$  Cal yrs B.P. and is capped by a section of silty sediments. The foraminiferal assemblage in this section is dominated by *Ammonia* and *Elphidium* with a slight increase in agglutinated and common inner shelf taxa indicating a transition to outer bay (~0.5 m depth) and then inner shelf deposits (~0.15 m depth).

GC-5 penetrated central bay sediments capped by outer bay deposits (Fig. 10). The base of GC-5 contains medium-gray clayey-silt with shell fragments, and a single burrow (Fig. 10). Shell material from 2.92 m

depth has an age of  $8467 \pm 130$  cal yr B.P. and foraminifera are dominated by *Ammonia*. An interpolated age from the age model (Fig. 10B) indicates the central bay to outer bay transition occurred ~8.4 ka (~2.7 m depth). The outer bay sediments are comprised of medium-gray clayey-silt containing sporadic 2–4 cm-scale sandy layers that thicken toward the top of the core to decimeter scale layers with more shell fragments. From ~0.5–1.4 m depth there is an increase in foram fragmentation and sediments are dominated by *Elphidium*. Increasing diversity of foraminifera and presence of agglutinated forams beginning at 1.0 m depth to the top of the core indicate a gradual transition from outer bay depositional environment to modern day marine inner shelf. The peak in fragmentation at approximately 1.0 m depth coincides with a peak in dominance of *Ammonia* and suggests that the increase in *Ammonia* likely represents reworked material. The outer bay section contains mollusk shell fragments that were dated to  $8445 \pm 135$  cal yr B.P. at 2.50 m depth and  $6661 \pm 169$  cal yr B.P. at 0.73 m depth (near the top), indicating potential ages for these sediments.

#### 4.5. Gravity core 1

GC-1 is extremely short (0.35 m total length; Fig. 11). Its location was selected to investigate dipping reflectors seen in seismic data hypothesized to be a Holocene-aged point bar deposit of a tributary at the edge of the Trinity Paleovalley (Fig. 11). Instead, the core penetrated a Pleistocene-age terrace containing sticky, dense, burrowed Beaumont Clay. This clay is capped by burrowed sand and thick shell hash and has a sharp contact with modern inner shelf deposits at approximately 0.14 m depth (Fig. 11C). Foraminiferal analysis revealed a large population of foraminifera, dominated by *Elphidium*, within one of the burrows of the terrace (see Appendix A). Carbon dating of these foraminifera tests revealed an age of  $38,081 \pm 1833$  cal yr B.P. almost certainly owing to the inclusion of older material, potentially in the form of dissolved inorganic carbon from the Beaumont Clay. Samples at the terrace contact (0.14 m depth) contained populations of foraminifera dominated by *Ammonia*. Sediments above the terrace contact were dominated by both *Elphidium* and *Ammonia* with a slight increase in agglutinated forams and a prominent increase in inner shelf genera, indicating a modern marine environment.

To test radiocarbon dating of different calcium carbonate material, we selected a mollusk shell from the same sample interval as foraminiferal tests for radiocarbon dating (0.05 m depth). The foraminifera provided an older age of  $1753 \pm 143$  cal yr B.P. than the mollusk shell, which was dated to  $589 \pm 97$  cal yr B.P. The difference in the ages may be the result of multiple processes: an amalgamation of material in a condensed section on the sediment-starved modern shelf; the presence of sediments containing detrital carbonate within the foram tests resulting in an older age; or perhaps diagenetic alteration of the foram tests, with recrystallization of pore water carbonate incorporating older material on the foraminifer tests, which have a higher surface area to mass ratio than the mollusk shells. Regardless, both ages indicate a much younger age for the 14 cm thick open shelf deposit (Fig. 11C) than any of the estuary sediments in the river valley. Seismic data at this location show prominent draping of sediments along the edges of the terrace (Fig. 11A), and a spike in fragmentation of foram tests coincides with the contact between the terrace and modern deposition (0.14 m depth), indicating a more significant amount of reworking at the contact.

#### 4.6. Gravity core 2

GC-2's location was chosen to identify a set of dipping reflectors believed to be part of a tidal delta (Fig. 12A). The core consists primarily of medium-gray clayey-silt with numerous layers of silty sand (Fig. 12). The lower part of the core (~2.0–3.6 m depth) contains foraminifera approximating 50–50 *Ammonia* and *Elphidium*. This assemblage combined with the increased sand content and the relatively higher percent of foram test fragmentation indicate this section likely contains tidal



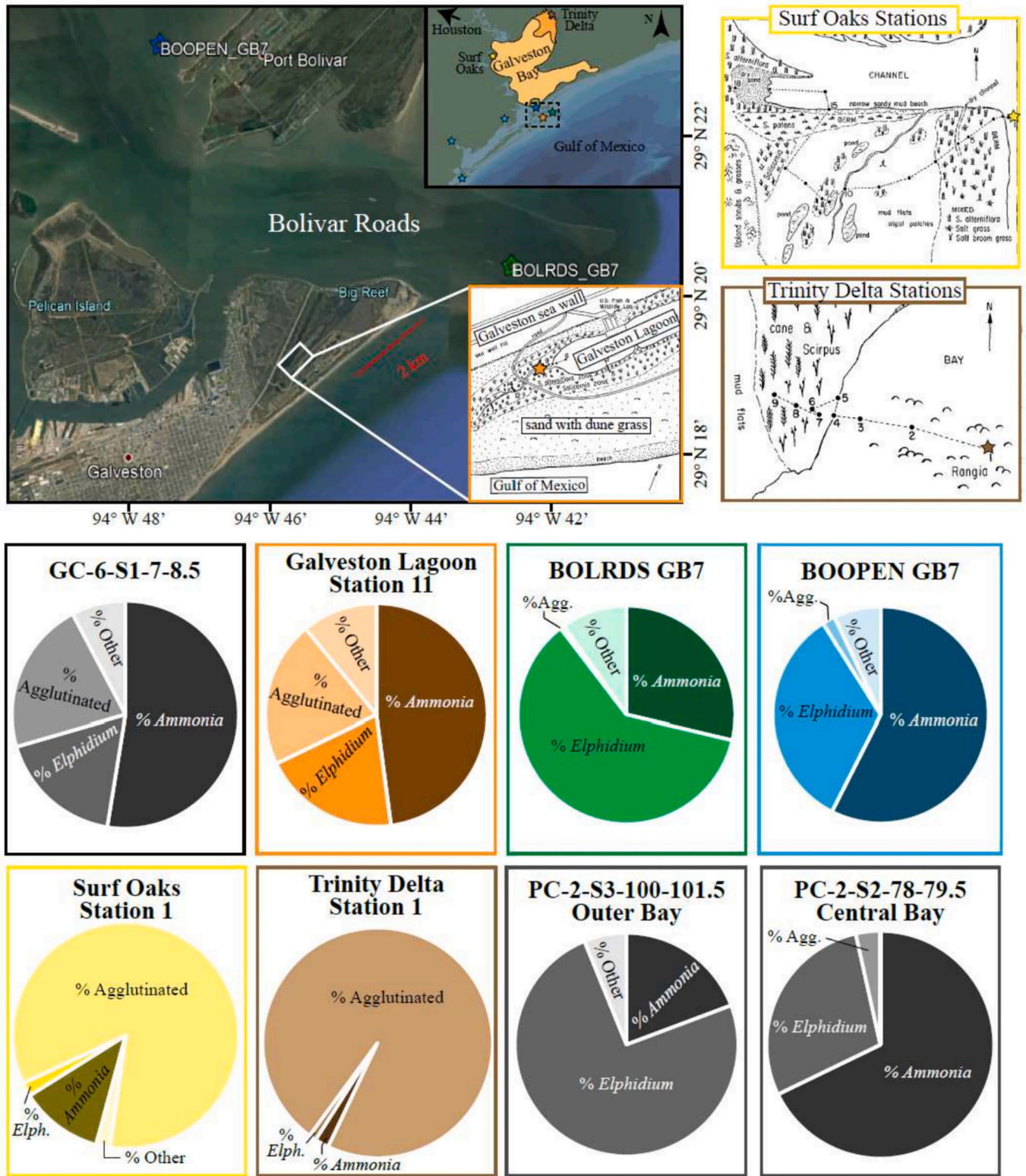
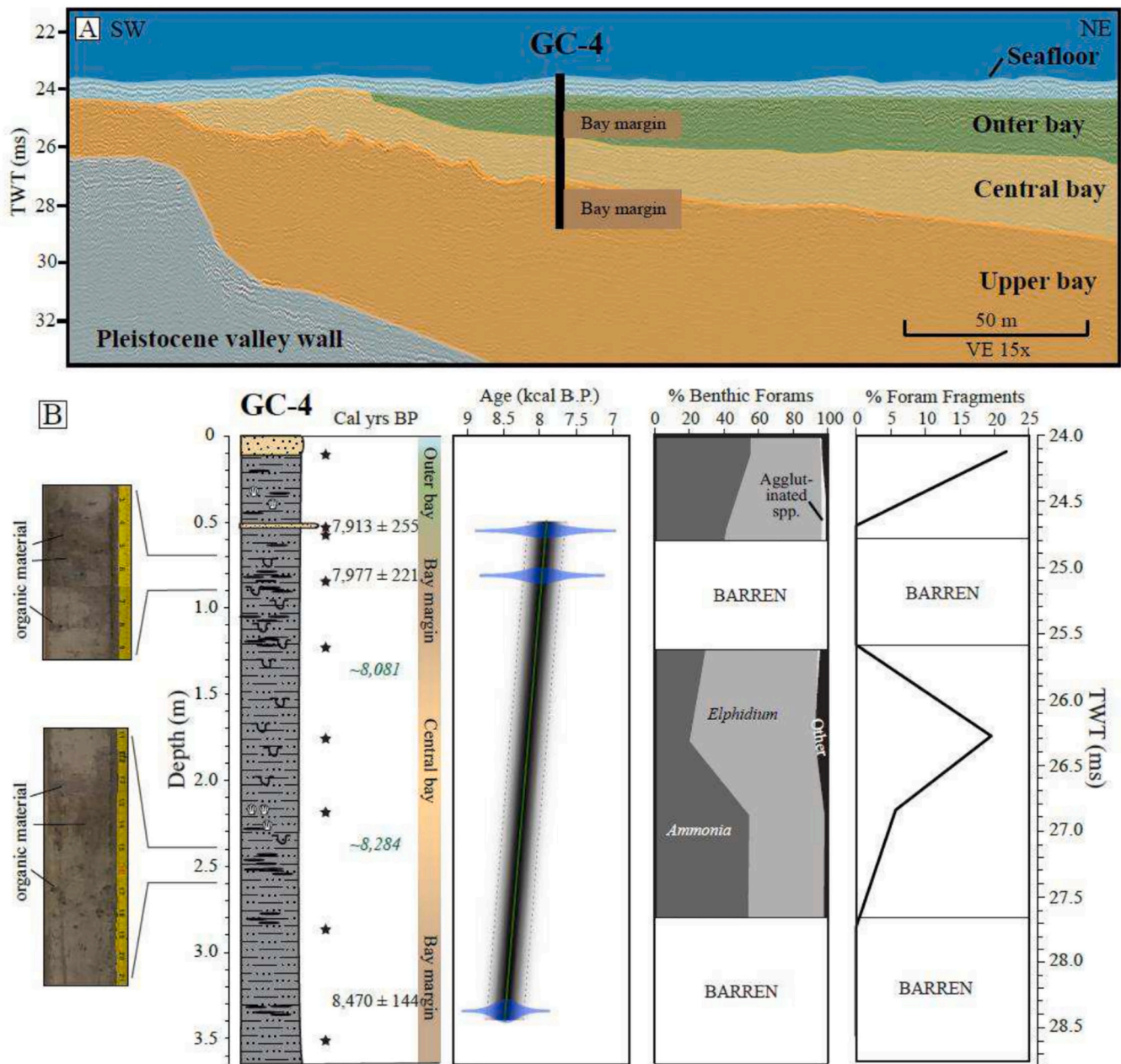


Fig. 8. Comparison of GC-6 upper sample (7–8.5 cm) to modern foram assemblages: Galveston Lagoon Station 11 (orange), Surf Oaks Station 1 (yellow), and Trinity Delta Station 1 (brown) analyzed by Phleger (1965); BOLRDS GB7 grab sample taken from the outer edge of the tidal inlet (green); BOOPEN GB7 grab sample taken from the inner edge of the tidal inlet (blue); and two samples from PC-2 representing the outer bay and central bay sediments (grayscale). The Phleger (1965) station samples come from saltmarsh locations surrounding Galveston Bay, with Galveston Lagoon as the most seaward station located on Galveston Island, Surf Oaks on the western edge of the bay, and Trinity Delta as the most landward station. The Station 11 sample is the closest approximation to the GC-6 sample. Basemap image source Google Earth (2021); drawn maps of marsh locations from Phleger (1965). (For interpretation of the references to colour in this figure legend, the reader is referred to the web version of this article.)



**Fig. 9.** Gravity Core 4. A) Interpreted seismic data with approximate depth of penetration for GC-4 (location in Fig. 1), overlain by paleoenvironment based on micropaleontologic data, including intervals interpreted as bay margin based on lack of foraminifera in core sediments. Seismic interpretation from Burstein et al., 2023 (VE = vertical exaggeration). B) Partial core images and full stratigraphic column of GC-4 showing samples (black stars) with radiocarbon ages (black text), interpolated ages (italicized green text) from age model. Age model based off of radiocarbon ages (blue ovals tapering to error range), with mean age depicted by solid green line and gray scale out to 95% confidence interval predicted by the model. Interpreted depositional facies based off of foraminiferal assemblage abundances and percent foram fragments. Two-way travel time scale for stratigraphic column in ms calculated from approximate seismic velocity of 1525 m/s starting at time of seafloor. (For interpretation of the references to colour in this figure legend, the reader is referred to the web version of this article.)

delta deposits. Because it is capped by a less-sandy section dominated by *Elphidium* indicating an outer bay environment (~0.4–2.0 m depth), the base of the core is interpreted as a flood-tidal delta. Carbon dates from mollusk shells obtained near the transition from tidal delta to outer bay at 2.07 m depth and 2.19 m depth provide ages of  $8445 \pm 135$  cal yr B.P. and  $8546 \pm 173$  cal yr B.P., respectively. The top of the core (0.4 m depth) contains a spike in *Ammonia* coupled with an increase in fragmentation. Similar to GC-5, coincident increase in fragmentation with a spike in *Ammonia* likely represents a reworking of central bay material in the outer bay environment. The transition to modern inner shelf deposition begins at ~0.5 m depth (~7.0 ka), represented by the increase in

foraminiferal diversity and presence of agglutinated foraminifera.

### 5. Discussion

The coring locations in this study were chosen to sample specific seismic facies and were not intended to provide a cross-section down the Holocene estuary. However, the data can provide several short cross sections along strike in the proximal, middle, and distal parts of our study area generating a composite picture of the nature and timing of environmental change across this part of the estuary from its initial flooding ~10 ka to its continued evolution by ~6 ka. An analysis of the



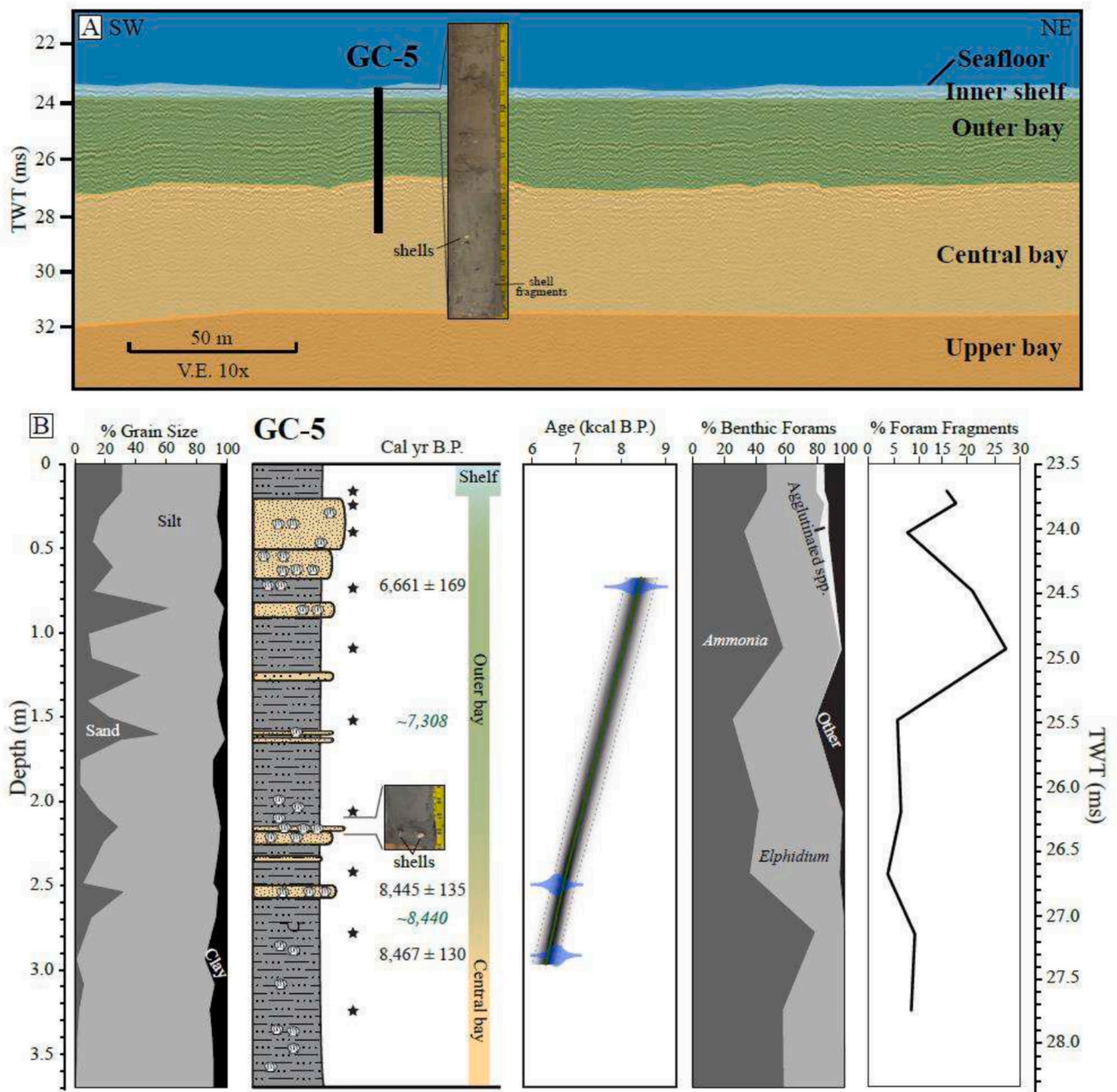


**Fig. 10.** Gravity Core 5 (GC-5). A) Interpreted seismic data with approximate depth of penetration for GC-5 (location in Fig. 1), overlain by paleoenvironment based on micropaleontologic data, and core image of sandy outer bay and inner shelf sediments. Seismic interpretation from (Burstein et al., 2023) (VE = vertical exaggeration). B) Grain size abundance and stratigraphic column of GC-5 with core image of sandy sediments and shell fragments and samples (black stars) with radiocarbon ages (black text), and interpolated ages (italicized green text) from age model. Age model based off of radiocarbon ages (blue ovals tapering to error range), with mean age depicted by solid green line and gray scale out to 95% confidence interval predicted by the model. Interpreted depositional facies based off of foraminiferal assemblage abundances and percent foram fragments. Two-way travel time scale for stratigraphic column in ms calculated from approximate seismic velocity of 1525 m/s starting at time of seafloor. (For interpretation of the references to colour in this figure legend, the reader is referred to the web version of this article.)

cores across the incised valley combined with interpolated ages from the age models shows consistent paleoenvironmental changes across multiple cores (Fig. 13), some of which coincide with events along the Texas Gulf Coast (Fig. 14; e.g., Anderson et al., 2022; Anderson et al., 2016; Anderson and Rodriguez, 2008; Simms et al., 2010; Troiani et al., 2011). The most landward part of this cross-section (Fig. 13, A-A'; Figs. 5 & 6) shows that PC-2 and PC-4 both transition from fluvial/terrestrial environments to upper bay at the same time (~9.8 ka); however, the

extrapolated age model date for PC-4 is not conclusive that the transition occurred simultaneously at both locations. Additionally, PC-2 and PC-4 do not transition from upper bay to central bay environments at the same time (PC-2 at ~9.6 ka and PC-4 at ~8.8 ka), likely due to the elevation of the Pleistocene terrace at PC-4's location. Subsequent environmental changes along this profile appear to occur simultaneously. PC-2, PC-4, and GC-6 all transition from central bay to outer bay environments at approximately the same time - 8.2-8.0 ka.



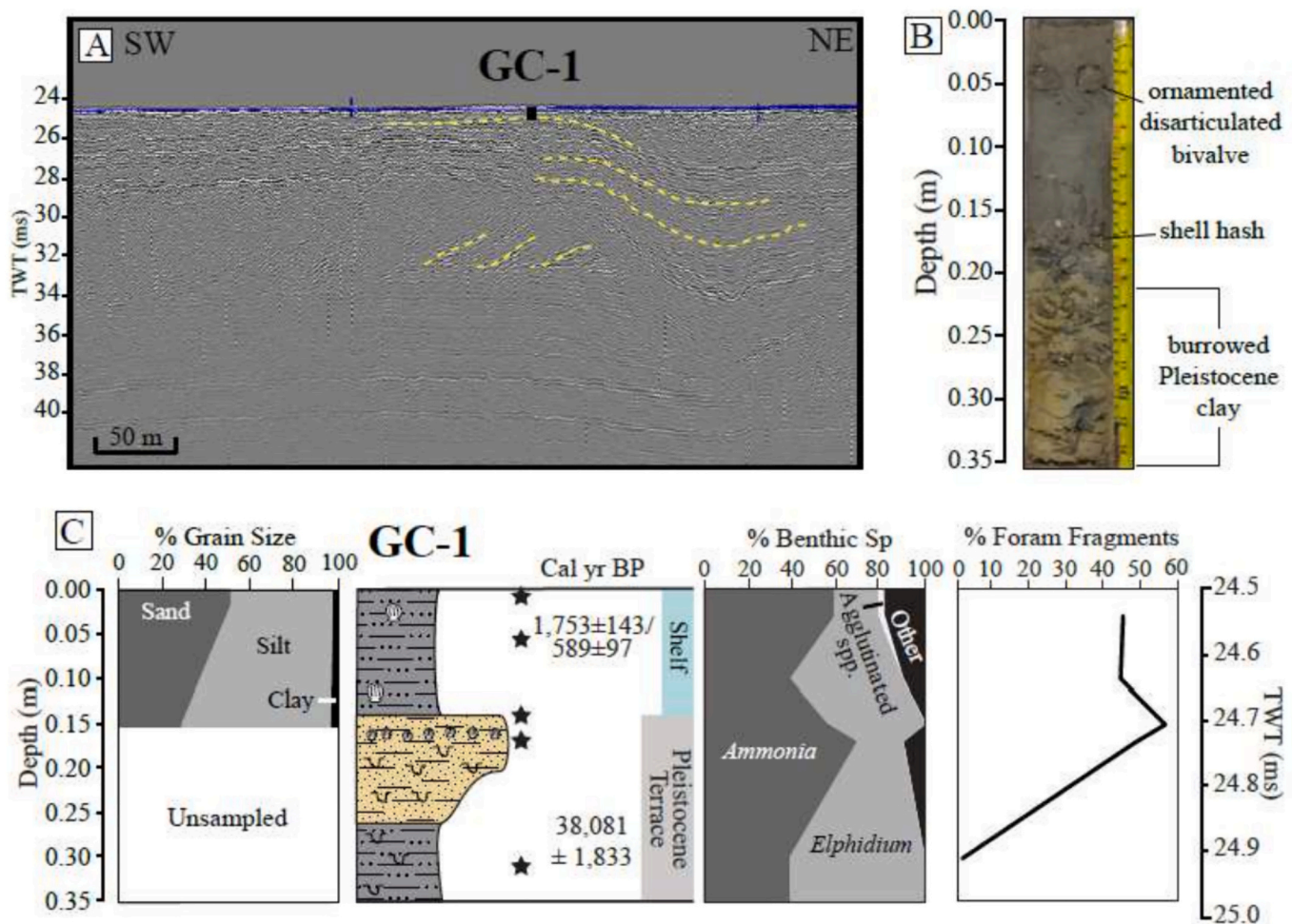


**Fig. 11.** Gravity core 1 (GC-1). A) Uninterpreted seismic line showing location of GC-1 short core where it penetrated a high-elevation Pleistocene terrace. Yellow dashed lines show approximated interpretation of draped sediments and dipping reflectors. B) Image of entire core. C) Grain size abundance (only upper 15 cm of core sampled for grain size) and stratigraphic column of GC-1 showing sample locations (black stars), radiocarbon dates, and interpreted depositional environments based on lithology, and foraminiferal assemblages and fragmentation. Two-way travel time (TWT) scale calculated based on approximate seismic velocity of 1525 m/s starting at time of seafloor. (For interpretation of the references to colour in this figure legend, the reader is referred to the web version of this article.)

Similarly, GC-2 (Fig. 13, C-C') and GC-5 (Fig. 13, B-B') show a coincident transition to outer bay environment at  $\sim 8.4$  ka; however, GC-4 does not transition to an outer bay environment until  $\sim 7.9$  ka. In general, outer bay sediments show a seaward thickening sequence from PC-2's location (Fig. 13, D-D').

Additionally, all cores in the study area, except for GC-6, appear to transition to an inner shelf environment beginning at  $\sim 6.9$  ka. Although this interval is difficult to date because of erosion of material during transgression and the limited inner shelf sediments observed in all cores (Fig. 14C), coincident timing suggests that the paleoestuary was relatively stable and changes in shoreline position and/or lateral shifts in the position of the tidal inlet led to the observed environmental transitions. Overall, the lateral differences in sediments within the cores reflect contemporaneous estuarine environmental variability.

Micropaleontologic evidence from these cores confirms the existence of a long-term stable estuarine environment; however, the seaward boundary of this estuary is not well-constrained with the existing dataset (Fig. 15), and further research on the seaward side of our study area is needed to determine when and where this boundary shifted. Approximately 9.8–9.6 ka, a large estuary stretched from the modern shoreline of Galveston Bay to seaward of Heald Bank (Fig. 15a). The flood-tidal delta at the base of GC-2 indicates that, in the vicinity of the Trinity River Paleovalley, the shoreline shifted landward of Heald Bank by at least 8.8 ka (Fig. 15b). In particular, our data suggest the paleoestuary

was present landward of Heald Bank for  $\sim 2$  kyr ( $\sim 8.8$ – $6.9$  ka) with some tidal inlet changes that altered the environment within the estuary without evidence of shoreline transgression (Fig. 15a-c, Burstein et al., 2023). In contrast, Rodriguez et al. (2004) concluded that the shoreline was approximately at Heald Bank's location at  $\sim 7.7$  ka. These apparently contradictory observations could be reconciled if, as Rodriguez et al. (2004) postulated for the 5.3 ka shoreline, the 7.7 ka shoreline also exhibited a significant bend or step (Fig. 15d). While such a geometry may seem unrealistic, the southern end of Assateague Island and its transition to Wallops Island, on the Eastern Shore of Virginia on the US Atlantic Coast, is a possible modern analog for such a formation.

Although we have mapped the estuarine sediments within the bounds of the Trinity River incised paleovalley (Fig. 15), it is possible that the estuary extended beyond the paleovalley, just as it does in the modern setting, and any estuarine sediments to the east and west of our study area have been removed during transgressive erosion. A subsequent landward shift took place  $\sim 6.9$  ka when the barrier system transgressed to a location between GC-2 and GC-5 (Fig. 15d). This shift was followed by additional landward barrier migration. The age of this later transgression cannot be determined in our cores because of the erosion of material as the shoreline passed across our study area. Transgressive lag deposits in GC-6 combined with overlying inner shelf environment of the cores, indicate the shoreline was landward of our study area by at least 4.3 ka (Fig. 15e-f). This is consistent with previous

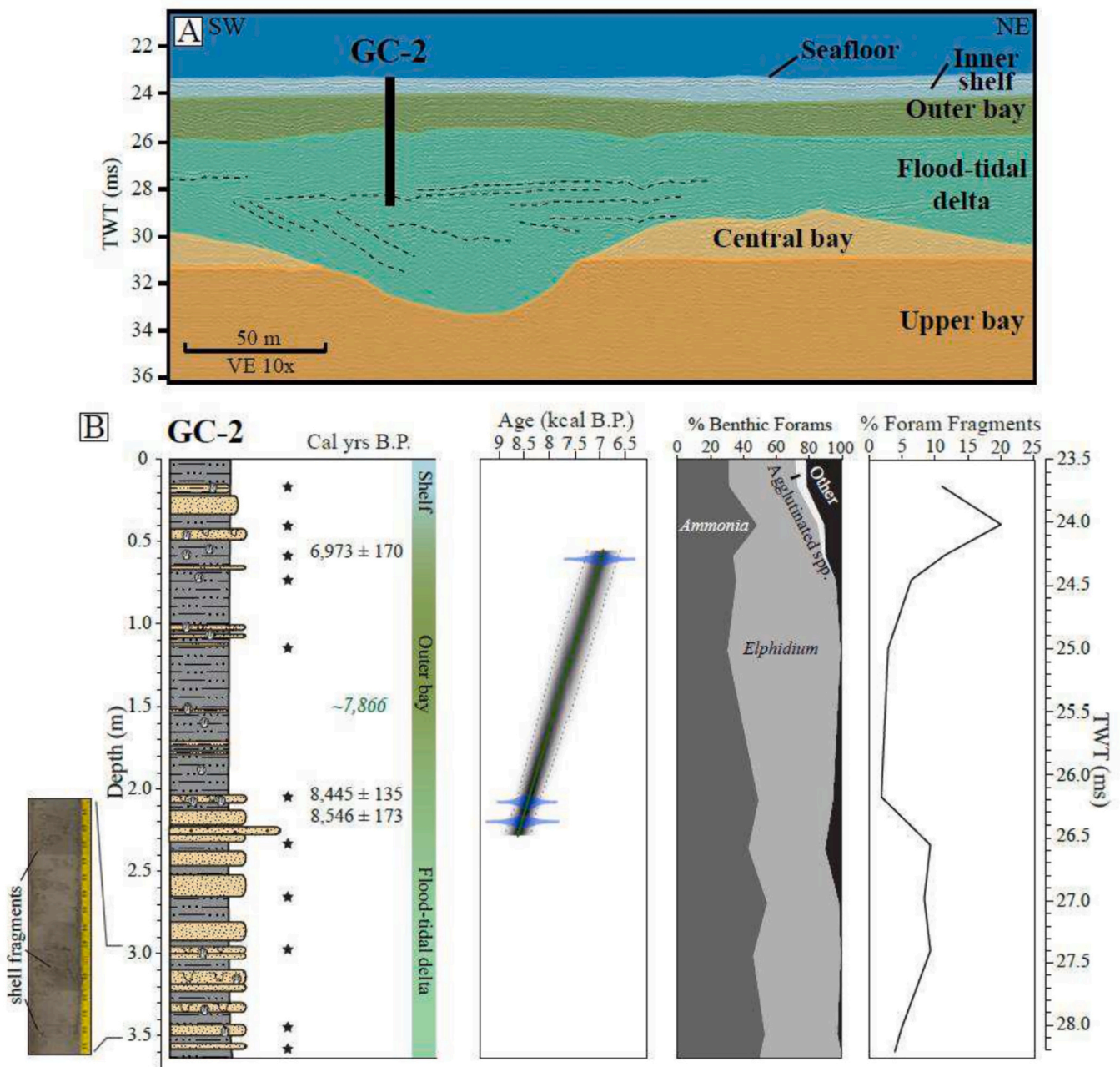


**Fig. 12.** Gravity core 2 (GC-2). A) Interpreted seismic data with approximate depth of penetration for GC-2 (location in Fig. 1), overlain by paleoenvironment based on micropaleontologic data. Seismic interpretation from Burstein et al. (2022) (VE = vertical exaggeration). B) Partial core image and full stratigraphic column with sample locations (black stars), radiocarbon dates (black text), interpolated ages (italicized green text) from age model. Age model based off of radiocarbon ages (blue ovals tapering to error range), with mean age depicted by solid green line and gray scale out to 95% confidence interval predicted by the model. Interpreted depositional facies based off of foraminiferal assemblage abundances and percent foram fragments. Two-way travel time scale for stratigraphic column in ms calculated from approximate seismic velocity of 1525 m/s starting at time of. (For interpretation of the references to colour in this figure legend, the reader is referred to the web version of this article.)

studies (e.g., Anderson et al., 2008; Rodriguez et al., 2004), which, based on radiocarbon dating of beach ridges, conclude that the shoreline reached its modern location on Galveston Island by ~5.3 ka on the western side (15e-f) (Anderson et al., 2022; Rodriguez et al., 2005).

5.1. Stable paleoestuary

Extensive research conducted by the Anderson group argues for the existence of >75 km long paleoestuary from Heald Bank ~50 km offshore Galveston Bay to the modern bay between ~8.2–7.8 ka (Fig. 3) (Anderson et al., 2008; Rodriguez et al., 2004). This evidence includes

seismic data and carbon dating of sediment cores from within modern Galveston Bay and Heald Bank (Anderson et al., 2008; Rodriguez et al., 2004).

Foraminiferal analysis from PC-2 and PC-4 indicates that both sites were located in the central bay from at least 8.8 ka to 8.0 ka, although PC-2 transitioned to a central bay environment by ~9.6 ka, confirming the existence of a long-term stable estuary (Figs. 5 & 6). Foraminiferal assemblages in PC-2 and PC-4 during this time period were dominated by *Ammonia* with common *Elphidium*, corresponding to a central bay depositional environment. Assemblages in PC-4 moving up through the core (2.7–1.3 m depth) show a decreasing abundance of *Ammonia* and an



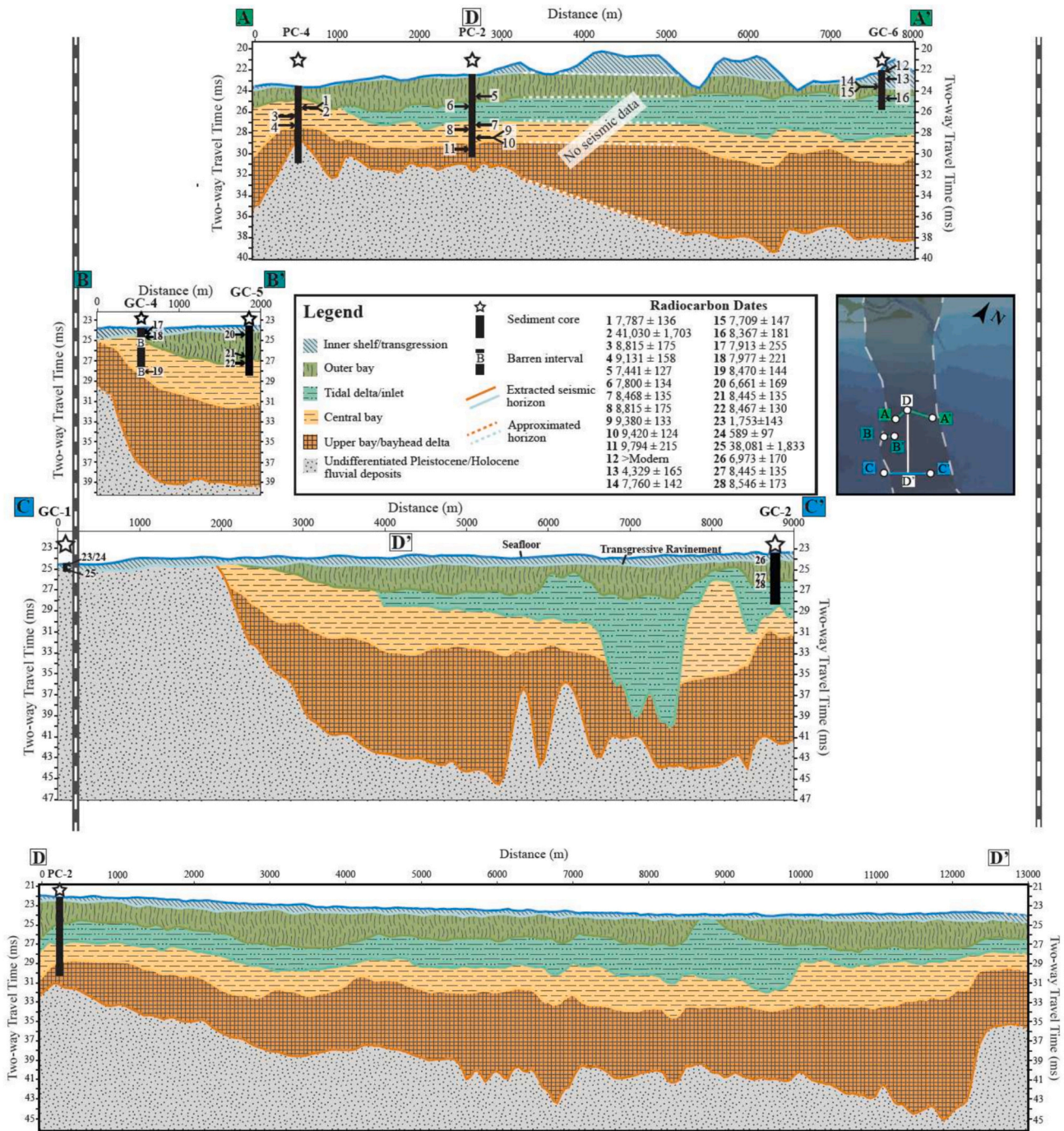


**Fig. 13.** Fence diagram showing depositional environment between cores within our study area. Depositional facies across the Trinity River Paleovalley are approximated from extracted seismic horizons in (Burstein et al., 2023). Horizons were interpolated for a portion of profile A-A' between PC-2 and GC-6 where there is no seismic data available. Core depths approximate from two-way travel time conversion using approximated velocity of 1525 m/s. Basemap for core and profile locations obtained from Global Multi-Resolution Topography Data Synthesis (Ryan et al., 2009) via GeoMapApp ([www.geomapp.org](http://www.geomapp.org)).

increase in *Elphidium* over time indicating a gradual environmental transition from upper bay to central bay and to outer bay. However, higher resolution analysis of PC-2 shows fluctuations in *Ammonia* and *Elphidium* abundances throughout the entire central bay interval, which may correspond to salinity fluctuations within the Holocene estuary as tidal inlets changed shape and/or location, or perhaps as precipitation in the catchment varied. This suggests that although environmental variability occurred within the paleoestuary, the outer boundaries remained stable enough to maintain a central bay environment. Additionally, many of the peaks in *Ammonia* correspond to small increases in foram

fragmentation (e.g., 3.4 and 3.7 m depth), which may indicate reworking of central bay material during that interval. The PC-2 analysis shows that portions of the estuary experienced marine mixing at ~8.4 ka (Fig. 5B) coinciding with a transition of seaward core locations to outer bay environments (Fig. 13, B-B' & C-C'). Increased marine influence on the estuary may provide an explanation for the small variations in foraminiferal assemblages observed in the middle estuary. Despite these marine incursions, the paleoestuary was likely protected due to the formation of barrier islands in the paleovalley (Burstein et al., 2023).

GC-4 is located at the western edge of the paleovalley and contains



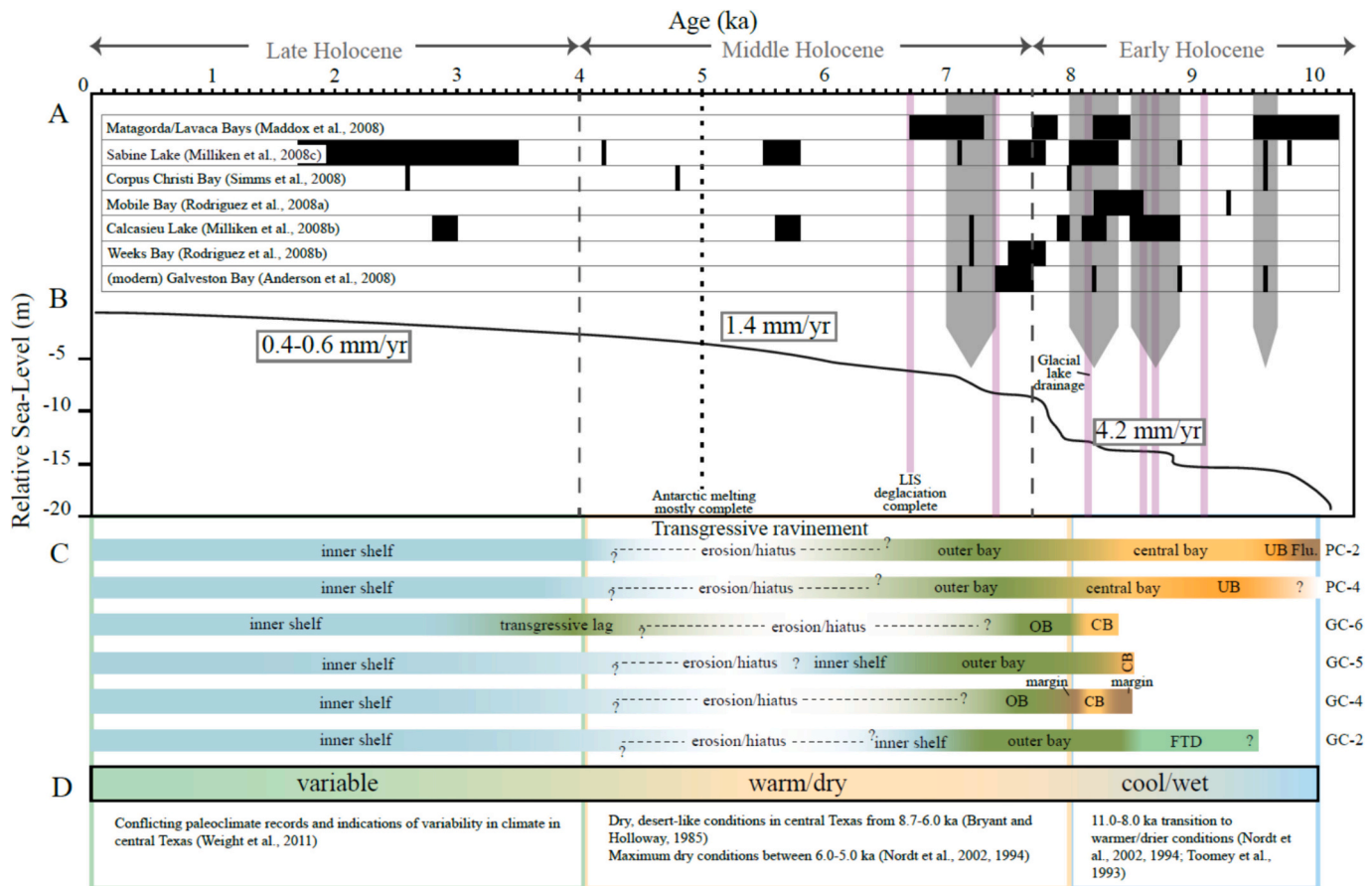


**Fig. 14.** Timeline of environmental change and sea-level rise in Galveston paleoestuary. A) Flooding events from other Gulf Coast Bays. B) Gulf Coast Holocene sea level curve (modified from Milliken et al., 2008a) containing prominent North American glacial events (purple) identified in Jennings et al. (2015), northern Gulf of Mexico flooding events (gray) from Milliken et al. (2008a), and rates of sea-level rise for the early, middle, and late Holocene (boxed in gray) from Anderson et al. (2022). C) Compilation of environmental change within Trinity River paleovalley cores for our study area and approximated period of transgressive erosion. D) Gulf Coast dominant climate regimes for the Holocene (modified from Weight et al., 2011). A majority of environmental transitions take place during a cool/wet climate when sea-level rise was more rapid, while significant transgressive erosion took place during a warm/dry period when sea-level rise slowed. (For interpretation of the references to colour in this figure legend, the reader is referred to the web version of this article.)

sediment and foraminiferal assemblages that record lateral variation in the boundary of the estuary between ~8.2 ka and ~8.1 ka (Figs. 9 and 13). While it is difficult to pinpoint the exact forcing mechanism for this expansion with existing evidence, it coincided with an environmental transition in GC-6. This suggests that the western boundary of the paleoestuary expanded due to sea-level rise prior to probable partial barrier collapse/rollover and the transition to an outer bay seen first in GC-6 and subsequently in PC-2 and PC-4 (Fig. 13). Although this expansion may have impacted the stability of the barrier system, it is unlikely that the shoreline changed significantly based on the maintenance of an outer bay environment during this time at GC-2's location (Fig. 12) and the existence of tidal delta deposits identified by Thomas and Anderson (1994) (Fig. 15). High-resolution seismic data in our study area show that antecedent fluvial highs probably provided a pinning point for the barrier system to stabilize at, which likely protected the paleoestuary during periods of rapid sea-level rise (Burstein et al., 2023).

### 5.2. Paleoshoreline changes

Rodriguez et al. (2004) describe estuarine muds in Heald Bank cores that were dated to 8015 ± 50 and 7770 ± 65 yr ago (both from articulated *Mulinia lateralis* bivalves) and suggested that the paleoshoreline was at Heald Bank ~7.77 ka. Due to the limited preservation of barrier islands offshore in the sediment record, we must infer original island

locations or areas of development based on the sediments that are preserved. Tidal inlet and tidal delta deposits are considered evidence for the presence of barrier systems that are not preserved (Anderson et al., 2016). Analysis of GC-2 reveals the existence of flood tide delta deposits dated to before ~8.5 ka, indicating that the inlet (and thus the barrier island system) was nearby (Fig. 12) (Burstein et al., 2023). Likewise, the presence of sandy deposits in GC-5 at ~6.7 ka and GC-6 at ~4.3 ka potentially demonstrates the landward migration of the paleoshoreline as sea level continued to rise throughout the Holocene (Fig. 16). Both GC-2 and GC-5 transition to outer bay environments by ~8.4 ka (Figs. 10 & 12), indicating that the outer boundary of the estuary within the Trinity River Paleovalley shifted and/or the paleobarrier system collapsed/rolled over prior to the transition to what are described as sandy shoreface deposits in Heald Bank cores (Rodriguez et al., 2004). As noted above, these observations could be reconciled if, as Rodriguez et al. (2004) postulated for the 5.3 ka shoreline, the 7.7 ka shoreline also exhibited a significant bend or step (Fig. 15d).

Sandy deposits in the outer bay sequence of GC-5 are probable washover sediments from a proximal barrier island. The absence of these sands in the bay margin intervals of GC-4 (Fig. 9) indicate that these washovers are not from the edge of the bay, westward of GC-5's location (Figs. 10 & 13). We hypothesize that a barrier system developed near GC-5's position ~20 km seaward of the modern shoreline ~6.7 ka (Fig. 15). Sandy intervals in the outer bay section of GC-2, located seaward of GC-5, containing a shell with an age of 6973 ± 170 cal yr B.P.

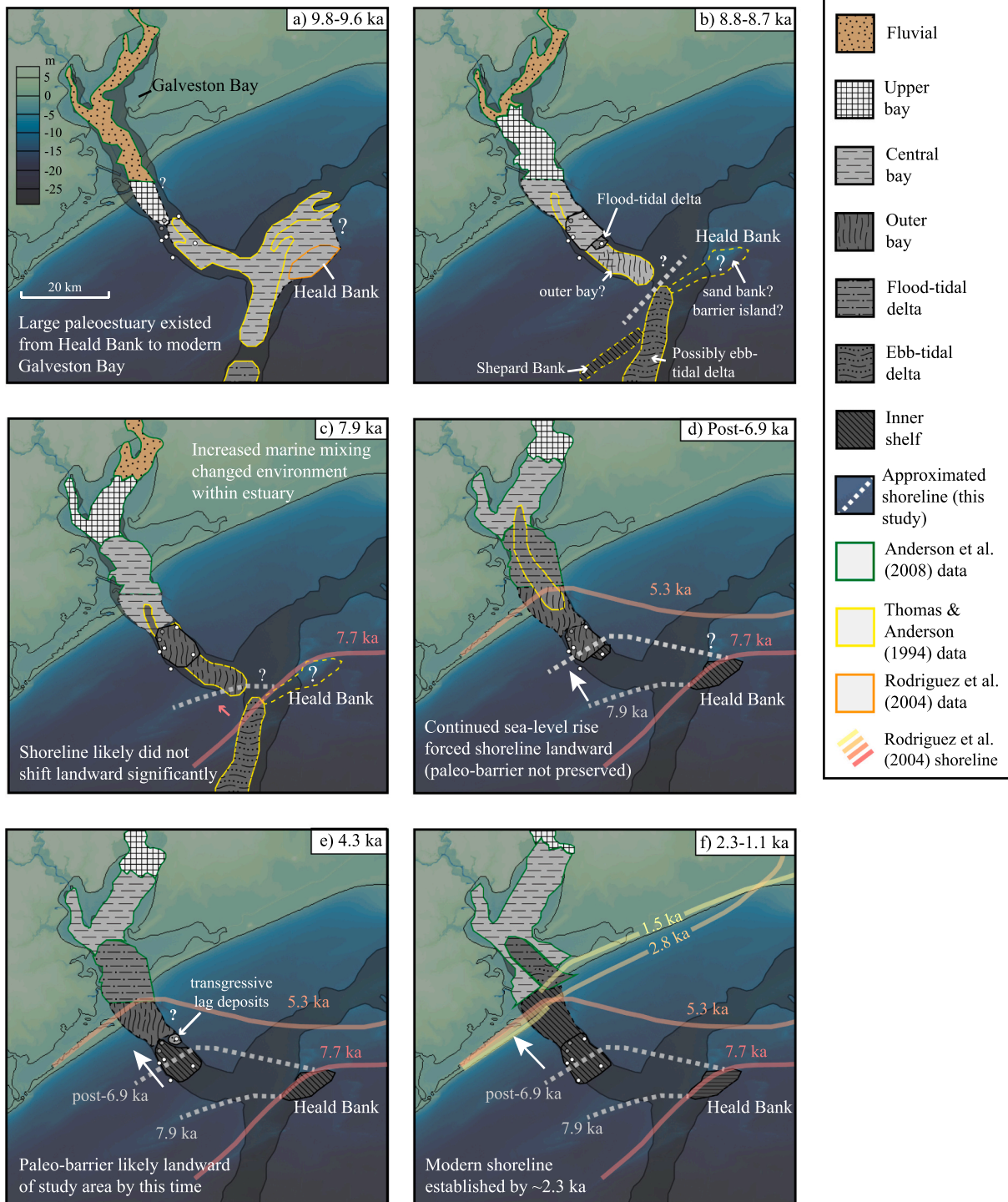


**Fig. 15.** Summary of paleoenvironmental change of Holocene estuary offshore Galveston Bay, Texas. Environmental facies at specific periods of time are based on micropaleontological analysis of cores in study areas and combined with previous research (outlined in green, yellow, and orange), and inferences were made between these study areas (dashed outlines). Facies are mapped within the bounds of the incised valley, but likely extended beyond those boundaries; however, the outer boundaries are difficult to determine due to probable removal of sediments during marine transgression. Paleoshorelines are estimated based on proximity to tidal delta and outer bay environments, and identification of probable washover sediments in cores. (For interpretation of the references to colour in this figure legend, the reader is referred to the web version of this article.)

also suggest that a barrier had developed nearby in the seaward direction, and these sandy intervals could represent paleo-storm/washover deposits from that barrier system.

In addition to the data provided in GC-2 and GC-5, transgressive lag deposits in GC-6 (Fig. 7) suggest that there was a barrier system proximal to GC-6's location between ~7.4 and 4.3 ka (Fig. 15). The upper

sample obtained from GC-6 closely resembles a modern marsh assemblage from Galveston Island (see 4.3), indicating that these sandy deposits could be from either a back-barrier marsh or a marsh located on the edge of the paleoestuary, and are not remnant ebb-tidal delta deposits (Fig. 8). Although we cannot confirm the timing and location of a paleobarrier near GC-6 with our current dataset, the foraminiferal

assemblage identified at the top of the sandy sediments can only be explained as originating from a back-barrier marsh. Additionally, the lack of organic material in the sandy sediments suggests that these sediments are not from a relict barrier island but have been reworked from a backbarrier marsh environment.

Analysis of Galveston Island core data by Rodriguez et al. (2004), coupled with previous research on the island by Bernard et al. (1970), indicates that Galveston Island began prograding ~5.3 ka giving the paleoshoreline an irregular shape and showing rapid, rather than gradual, coastline changes in the past (Figs. 2 & 15). Although coastal changes typically adjust to sea-level rise “dynamically while maintaining a characteristic geometry that is unique to a particular coast” (FitzGerald et al., 2008, p. 601), it is likely the irregular depth of the Holocene-Pleistocene surface on either side of the Trinity River paleovalley (Fig. 2) is the cause for this oblique paleoshoreline change (Rodriguez et al., 2004). Based on probable washover and transgressive lag sediments reported here, the paleoshoreline east of Galveston Island’s location likely stepped landward multiple times until reaching its modern-day location by ~2.5 ka; however, the lack of data between our study area and the modern shoreline makes it difficult to constrain this migration beyond the proximity of the shoreline to GC-6 at ~4.3 ka.

### 5.3. Timeline of sea-level rise

Estimates of Antarctic ice-sheet fluctuations since the Last Glacial Maximum vary widely, so most Holocene sea-level rise is attributed to the better constrained demise of the Laurentide Ice Sheet (Lambeck et al., 2014); however, initial retreat of the West Antarctic and Antarctic Peninsula Ice Sheets began between 15.0 and 12.0 ka with significant retreat in the Ross and possibly Weddell Seas after 7.0 ka (Anderson et al., 2002) and a more recent synthesis of Antarctic Holocene deglaciation indicates that a majority of melting occurred by or shortly after 5 ka (Bentley et al., 2014). Higher resolution analysis of Laurentide Ice Sheet deglaciation reveals multiple meltwater pulses at 9.1 ka, 8.7 ka, 8.6 ka, 8.2 ka, and 7.4 ka (Cronin et al., 2007; Jennings et al., 2015; Törnqvist et al., 2004; Ullman et al., 2016). After 8.15 ka, Laurentide Ice Sheet retreat accelerated with remnant ice domes melting by ~6.7 ka (Lambeck et al., 2014; Ullman et al., 2016). Remaining global sea-level rise is attributed to the loss of ice volume from the West Antarctic ice-sheet during the late Holocene (Ullman et al., 2016).

While many of these pulses can be connected to rapid environmental change along the Gulf Coast, some events are more likely due to the impact of antecedent geology (Anderson et al., 2014; Burstein et al., 2023) and/or regional climate changes impacting sediment supply (Anderson and Rodriguez, 2008). A comparison of environmental changes in the paleoestuary and the record of Gulf of Mexico sea-level rise indicates that most of these transitions coincide with or occurred after periods of rapid increases in sea level, although some environmental shifts transpired after global sea-level rise slowed significantly, indicating other regional and local changes, such as hydroclimate, may have contributed to these transitions (Fig. 14).

Many of the environmental transitions in our study area correlate with flooding surfaces identified in other Gulf Coast bays, when the rate of sea-level rise was 4.2 mm yr<sup>-1</sup>, suggesting global sea-level rise played a dominant role. At 9.8 ka, PC-2 transitions from a fluvial to an upper bay environment. Inundation in the Galveston paleoestuary also coincides with the initial flooding of the Sabine-Neches incised valley (Milliken et al., 2008c) and a flooding surface in Matagorda/Lavaca estuary complex (Maddox et al., 2008). At ~9.6 ka, the estuarine setting at core site PC-2 transitioned from an upper bay to central bay environment (Figs. 5 & 14), shortly after flooding in the modern Galveston Bay that resulted in formation of a bayhead delta (Anderson et al., 2008). This generally coincided with initial flooding of Copano Bay (Troiani et al., 2011), and the landward stepping of the fluvial system in Sabine Lake (Milliken et al., 2008b). A drowning event of the Nueces River valley in Corpus Christi Bay at about this time may or may not

have been a rapid flooding event (Simms et al., 2008). These events likely resulted from sea-level rise caused by the retreat of the Antarctic Ice Sheet (Anderson et al., 2002) and are either within or just after a period of rapid sea-level rise identified by Milliken et al. (2008a). PC-4’s location transitioned from an upper bay to central bay environment at ~8.8 ka, coinciding with a period of rapid sea-level rise (Milliken et al., 2008) and a flooding event in Calcasieu Lake that shifted the bay shoreline landward (Milliken et al., 2008b) and shortly after flooding events in modern Galveston Bay (Anderson et al., 2008) and Corpus Christi Bay (Simms et al., 2008). The lack of longer cores in the seaward portion of our study area precludes our ability to determine if the outer boundary of the estuary shifted along with the paleoenvironmental changes at PC-2 and PC-4; however, previous analysis suggests that the paleoshoreline likely did not shift landward until barrier migration ~6.9 ka (Burstein et al., 2023).

There are a series of paleoenvironmental changes between 8.5 and 7.9 ka, likely in response to rapid sea-level rise events, in which the paleoestuary progressively transitions from a central bay to an outer bay environment. These changes partially coincide with a significant deglacial event, typically referred to as the “8.2 ka event,” in which a large glacial lake drained into the North Atlantic and led to short-term climate cooling (Cronin et al., 2007; Jennings et al., 2015; Törnqvist et al., 2004; Ullman et al., 2016). Other portions of the Texas Gulf Coast also experienced rapid flooding events likely as a result of global pulses of sea-level rise, including Matagorda/Lavaca estuary complex (~8.5–8.2 ka; Maddox et al., 2008), Copano Bay (~8.2 ka, Troiani et al., 2011), Baffin Bay (~8.0 ka, Simms et al., 2010), Mobile Bay (~8.7–8.2 ka; Rodriguez et al., 2008b), Sabine Lake (~8.4–8.0 ka; Milliken et al., 2008c), Calcasieu Lake (~8.3–8.0 ka; Milliken et al., 2008b), modern Galveston Bay (~8.2 ka; Anderson et al., 2008), and Corpus Christi Bay (~8.0 ka; Simms et al., 2008). There is also an increase in diversity of the foraminiferal population in PC-2 between 8.4 and 8.1 ka, possibly due to elevated salinity levels from a partial or total collapse/rollover of the barrier system as other portions of the paleoestuary transitioned more saline environments (Fig. 5). This also corresponds to the 8.2 ka flooding event observed elsewhere. Additionally, carbon isotope records show that between 11.0 and 8.0 ka, the central Texas region was transitioning to a warmer and drier climate (Nordt et al., 2002; Nordt et al., 1994), so it is likely that the drying hydroclimate reduced sediment supply, which contributed to these changes.

Slightly before 8.5 ka, foraminiferal populations within GC-2 (the most seaward core in our study area) exhibit an increase in inner shelf species (Fig. 12), suggesting a marine incursion at that location and the beginning of a landward migration of the Galveston paleoestuary. This is followed by a transition at ~8.5 ka in GC-2 from a flood-tidal delta environment to an outer bay environment, potentially demonstrating a stabilization in the barrier system (Fig. 12). At 8.4 ka, GC-5 transitioned to outer bay environments (Fig. 10), coinciding with landward migration of the river mouth in the Matagorda/Lavaca estuary complex (Maddox et al., 2008), rapid (~100 m yr<sup>-1</sup>) landward transgression of the bayline in Mobile Bay (Rodriguez et al., 2008b), and landward movement of the bayline in Sabine Lake (Milliken et al., 2008c). At 8.3 ka, sediments in GC-4 transition from a bay margin to a central bay environment (Figs. 9 & 14), interpreted as a sea-level rise event that expanded the boundaries of the paleoestuary. In addition to the above flooding events at ~8.4 ka, the GC-4 transition also coincided with a landward shift in the bayhead delta in Calcasieu Lake (Milliken et al., 2008b). At ~8.2 ka, within modern Galveston Bay, the bayline shifted ~10 km up the valley along with the landward migration of the bayhead delta (Anderson et al., 2008). Within our study area, the Galveston paleoestuary boundaries contracted ~8.1 ka and GC-6’s location transitioned to an outer bay environment (Fig. 7). By ~8.0 ka PC-2 and PC-4 both transitioned to an outer bay environment (Figs. 5 & 6), coincident with a rapid flooding event in Corpus Christi Bay in which the upper bay backstepped by 15 km in <200 yr and much of the modern bay became an open bay environment (Simms et al., 2008). Within the Galveston



paleoestuary, GC-4 transitioned to an outer bay environment at  $\sim 7.9$  ka (Fig. 9). Other changes along the Texas Gulf Coast include a landward shift of the delta within the Matagorda/Lavaca estuary complex between 7.9 and 7.7 ka and an expansion of Lavaca Bay followed by spit formation (Maddox et al., 2008), and a 10-km backstepping of the delta landward within Calcasieu Lake (Milliken et al., 2008b).

By 7.8 ka, all cores within our study area had transitioned to outer bay (Fig. 14). This was followed by an increase in inner shelf species within foraminiferal populations at PC-4 suggesting more marine conditions at that location (Fig. 5), a 10–20 km landward movement of the bayline in Sabine Lake (Milliken et al., 2008c), and initial flooding of the estuary in Weeks Bay (Rodriguez et al., 2008a). Although there are no changes within our study area between 7.7 and 7.4 ka, it is worth noting that sediments in the modern Galveston Bay show a flooding surface constrained to this time (Fig. 3) and landward migration of the bayhead delta and central bay (Anderson et al., 2008).

At  $\sim 7.3$  ka, shortly after a deglacial event and a regional climate shift to warmer and drier conditions, there is a brief increase in diversity in foraminiferal populations in GC-5 (Fig. 10), possibly associated with increased marine mixing, although there are no other indications of environmental change in other cores. This coincides with a dramatic change in the Matagorda/Lavaca estuary complex in which the bayhead delta shifted by 30 km between 7.3 and 6.7 ka, establishing the modern-day Matagorda Bay (Maddox et al., 2008).

After 7.0 ka, sea-level rise slowed to  $1.4 \text{ mm yr}^{-1}$  and the paleoestuary appears to have stabilized until marine transgression sometime between 6.7 ka and  $\sim 4.3$  ka, although that is difficult to pinpoint due to removal of material. The approximate timing of the transgressive ravinement overlaps with flooding surfaces in Sabine Lake (Milliken et al., 2008c), Calcasieu Lake (Milliken et al., 2008b), and Corpus Christi Bay (Simms et al., 2008). It is likely that a central Texas regional climate change from cool/wet to warm/dry conditions by  $\sim 8.0$  ka with peak warm/dry conditions around  $\sim 6.0$  ka (Fig. 14; Bryant and Holloway, 1985; Nordt et al., 2002; Nordt et al., 1994) contributed to these changes by reducing the sediment supply to the paleoestuary allowing for the landward migration of the paleoshoreline (Fig. 15). By  $\sim 5$  ka, Antarctic ice sheet melting was mostly complete (Bentley et al., 2014), after which our study environment stabilized as an inner shelf/open marine environment.

The influence of regional climate change, particularly hydroclimate, on paleoestuary stability suggests that modern warming, especially in combination with reduced precipitation, coupled with human-induced reduction in riverine sediment flux and subsidence may increase the vulnerability of Galveston Island and Bolivar Peninsula to accelerating sea-level rise. We are unable to determine the magnitude of change in sediment flux that resulted in previous shoreline retreat, as the only indication of this change is the mid-Holocene transition from a wet/cool to a warm/dry hydroclimate  $\sim 7.4$  ka and to a more variable climate  $\sim 4$  ka likely when our study area became inner shelf and the paleoshoreline was still in the process of migrating to its modern-day location (Figs. 14 & 15; Weight et al., 2011). Foraminiferal data indicates there were fluctuations in the estuarine environment while the shoreline was stable, suggesting alterations to salinity that may be due to hydroclimate changes or increased marine mixing from inlet changes. Additional study is required involving paleoclimate and paleoprecipitation changes in the Trinity River catchment to deduce how changes in sediment supply to the coast may have contributed to Holocene coastal change.

#### 5.4. Minimal modern seafloor sedimentation

The transition to a modern inner shelf environment is difficult to determine due to the limited amount of modern seafloor material and likely erosion and reworking of upper sediments from the transgressive ravinement. The only indication of the timing of transgression through our study area are radiocarbon dates of  $\sim 6.9$  ka in GC-2 and  $\sim 6.7$  ka in GC-5 prior to the transition from outer bay to inner shelf, and the

transgressive lag deposit in GC-6 containing a radiocarbon dated shell of  $\sim 4.3$  ka (Figs. 13–15). Based on these dates, it is likely that the transgression in our study area occurred over the period between 7.0 and 6.0 ka. The limited shelf material in the upper areas of each core represents deposition of  $\sim 0.01$  cm per year, so it is more likely that material is being removed from the upper seafloor regularly.

The Texas Mud Blanket is a large ( $\sim 300 \text{ km}^3$ ) depositional area on the western Gulf Coast between a bathymetric embayment of the ancient Rio Grande and Colorado River deltas containing  $\sim 5 \times 10^{11}$  t of sediment (Weight et al., 2011). It is likely that depletion of inner shelf sediments offshore Galveston Bay is the result of sediment remobilization via the Louisiana-Texas Coastal Current to regions farther west along the Texas Coast, including the Texas Mud Blanket.

## 6. Conclusion

We use new cores to refine the established Holocene coastal change model for the Trinity River incised valley based on new radiocarbon dates and micropaleontological analysis. This study provides environmental context to previous research that primarily utilized seismic and sedimentological analyses, revealing consistent environmental changes across multiple cores due to external sea-level rise and climate forcing. As a result of this analysis, we reach the following conclusions:

- Despite periods of rapid sea-level rise, the Galveston paleoestuary was relatively stable for approximately 2 kyr ( $\sim 8.8$ – $6.9$  ka) and experienced gradual environmental shifts within the paleoestuary associated with rapid sea-level rise events (e.g., the 8.2 ka event). Our data show that the paleoestuary experienced marine incursions and probable tidal-inlet migrations in otherwise stable outer boundaries that altered the paleoenvironment within the bay but did not collapse the paleoestuary entirely prior to full migration and marine transgression.
- Probable washover sediments approximate the location of barrier islands as they migrated landward at  $\sim 7$ – $6.7$  ka and after  $\sim 4.3$  ka. Data limitations preclude our ability to characterize how the barrier system may have migrated landward of our study area; however, based on previous analysis, the western side of the paleovalley was near its modern location by  $\sim 5.3$  ka and the eastern side migrated to its current location by  $\sim 2.5$  ka.
- Early Holocene paleoenvironmental changes coincide with previously identified flooding events in other Gulf Coast bays, suggesting global sea-level rise was a dominant cause of these changes. Subsequent middle to late Holocene paleoenvironmental transitions during reduced rates of sea-level rise were likely caused by regional hydroclimate change to warm and dry conditions that reduced sediment supply to the coast.
- All cores in the study area contain minimal modern seafloor sediments likely due to erosion from the transgressive ravinement and reworking of sediment from ocean currents contributing to the Texas Mud Blanket.

## CRediT authorship contribution statement

**P. Standing:** Writing – original draft, Visualization, Investigation, Funding acquisition, Formal analysis. **C.M. Lowery:** Writing – review & editing, Visualization, Supervision, Methodology, Investigation, Formal analysis. **J. Burstein:** Writing – review & editing; Investigation; Formal analysis. **J. Swartz:** Writing – review & editing; Investigation; Formal analysis. **J.A. Goff:** Writing – review & editing, Visualization, Supervision, Project administration, Investigation, Funding acquisition, Formal analysis. **S.P.S. Gulick:** Writing – review & editing, Visualization, Supervision, Project administration, Investigation, Formal analysis. **C.B. Miller:** Writing – review & editing, Visualization.

## Declaration of competing interest

The authors declare no conflict of interest.

## Data availability

Datasets related to this article can be found at <https://www.ncei.noaa.gov/access/paleo-search/study/34592>, an open-source online data repository hosted at NOAA's National Center for Environmental Information.

## Acknowledgments

This project was funded by the Bureau of Ocean Energy Management under Cooperative Agreement M16AC00020, and the Martin B. Lagoe Micropaleontology Fellowship from the Jackson School of Geosciences at the University of Texas at Austin. We would like to thank Gabriela Gutierrez, Daniel Duncan, Marcy Davis, the crew of the R/V *Brooks McCall*, TDI Brooks, the class of the 2018 Marine Geology and Geophysics Field Course, and the crew of the R/V *Manta* for their collective assistance in collecting the piston and gravity cores and additional chirp data for this study, and Nikki Bretting and Kate Gilbreath for assistance in grain size analysis. We would also like to thank the National Ocean Sciences Accelerator Mass Spectrometry at Woods Hole Oceanographic Institute (NSF Cooperative Agreement number OCE-0753487) for processing our radiocarbon samples, and the Gulf of Mexico Sedimentology Working Group for discussions contributing to the analysis presented in this paper. We acknowledge that research on this project was conducted at the University of Texas at Austin on the Indigenous lands of Turtle Island, on land originally cared for by the Alabama-Coushatta, Caddo, Carrizo/Comecrudo, Coahuiltecan, Comanche, Kickapoo, Lipan Apache, Tonkawa, and Ysleta del Sur Pueblo people, many of whom were forcibly removed from their home. For more information about ancestral land you occupy, please visit <http://native-land.ca/>. This is University of Texas Institute for Geophysics Contribution #3974.

## Appendix A. Supplementary data

Supplementary data to this article can be found online at <https://doi.org/10.1016/j.margeo.2024.107345>.

## References

- Abdulah, K.C., Anderson, J.B., Snow, J.N., Holdford-Jack, L., 2004. The late Quaternary Brazos and Colorado Deltas, Offshore Texas, U.S.A.—their Evolution and the Factors that Controlled their Deposition.
- Anderson, J.B., Rodriguez, A.B., 2008. Response of Upper Gulf Coast Estuaries to Holocene Climate Change and Sea-Level Rise. *Geological Society of America*.
- Anderson, J.B., Rodriguez, A.B., Milliken, K.T., Taviani, M., 2008. The Holocene evolution of the Galveston estuary complex, Texas: Evidence for rapid change in estuarine environments. In: Special Paper 443: Response of Upper Gulf Coast Estuaries to Holocene Climate Change and Sea-Level Rise. *Geological Society of America*, pp. 89–104. <https://doi.org/10.1130/2008.2443.06>.
- Anderson, J.B., Wallace, D.J., Simms, A.R., Rodriguez, A.B., Milliken, K.T., 2014. Variable response of coastal environments of the northwestern Gulf of Mexico to sea-level rise and climate change: Implications for future change. *Mar. Geol.* 352, 348–366.
- Anderson, J.B., Wallace, D.J., Simms, A.R., Rodriguez, A.B., Weight, R.W.R., Taha, Z.P., 2016. Recycling sediments between source and sink during a eustatic cycle: Systems of late Quaternary northwestern Gulf of Mexico Basin. *Earth Sci. Rev.* 153, 111–138.
- Anderson, J.B., Shipp, S.S., Lowe, A.L., Wellner, J.S., Mosola, A.B., 2002. The Antarctic Ice Sheet during the Last Glacial Maximum and its subsequent retreat history: A review. *Quaternary Science Reviews* 21 (1), 49–70. [https://doi.org/10.1016/S0277-3791\(01\)00083-X](https://doi.org/10.1016/S0277-3791(01)00083-X).
- Anderson, J.B., Wallace, D.J., Rodriguez, A.B., Simms, A.R., Milliken, K.T., 2022. Holocene Evolution of the Western Louisiana–Texas Coast, USA: Response to Sea-level rise and Climate Change. In: Anderson, J.B., Wallace, D.J., Rodriguez, A.B., Simms, A.R., Milliken, K.T. (Eds.), *Holocene Evolution of the Western Louisiana–Texas Coast, USA: Response to Sea-Level Rise and Climate Change*. *Geological Society of America*. [https://doi.org/10.1130/2022.1221\(01\)](https://doi.org/10.1130/2022.1221(01)).
- Bentley, M.J., Ó Cofaigh, C., Anderson, J.B., Conway, H., Davies, B., Graham, A. G.C., Hillenbrand, C.-D., Hodgson, D.A., Jamieson, S.S.R., Larter, R.D., Mackintosh, A., Smith, J.A., Verleyen, E., Ackert, R.P., Bart, P.J., Berg, S., Brunstein, D., Canals, M., Colhoun, E.A., Zwart, D., 2014. A community-based geological reconstruction of Antarctic Ice Sheet deglaciation since the Last Glacial Maximum. *Quaternary Science Reviews* 100, 1–9. <https://doi.org/10.1016/j.quascirev.2014.06.025>.
- Bernard, H.A., Major, C.F., Parrott, B.S., LeBlanc, R.J., 1970. *Recent Sediments of Southeast Texas—a Field Guide to the Brazos Alluvial and Deltaic Plains and the Galveston Barrier Island Complex*. University of Texas at Austin, Bureau of Economic Geology.
- Bernstein, A., Gustafson, M.T., Lewis, R., 2019. Disaster on the horizon: the price effect of sea-level rise. *J. Financ. Econ.* 134, 253–272. <https://doi.org/10.1016/j.jfineco.2019.03.013>.
- Blaauw, M., Christen, J.A., 2011. Flexible paleoclimate age-depth models using an autoregressive gamma process. *Bayesian Anal.* 6, 457–474. <https://doi.org/10.1214/11-BA618>.
- Bryant, V., Holloway, R., 1985. A late-Quaternary paleoenvironmental record for Texas: an overview of the pollen evidence. In: *Pollen Records of Late-Quaternary North American Sediments*, pp. 39–70.
- Burstein, J.T., Goff, J.A., Gulick, S.P.S., Lowery, C., Standring, P., Swartz, J., 2023. Tracking barrier island response to early Holocene Sea-level rise: High resolution study of estuarine sediments in the Trinity River Paleovalley. *Mar. Geol.* 106951 <https://doi.org/10.1016/j.margeo.2022.106951>.
- Buzas, M.A., 1990. Another look at confidence limits for species proportions. *J. Paleontol.* 2.
- Buzas-Stephens, P., Livsey, D.N., Simms, A.R., Buzas, M.A., 2014. Estuarine foraminifera record Holocene stratigraphic changes and Holocene climate changes in ENSO and the north American monsoon: Baffin Bay, Texas. *Paleoecol. Paleoclimatol. Paleoeconol.* 404, 44–56. <https://doi.org/10.1016/j.paleo.2014.03.031>.
- Cronin, T.M., Vogt, P.R., Willard, D.A., Thunell, R., Halka, J., Berke, M., Pohlman, J., 2007. Rapid sea-level rise and ice sheet response to 8,200-year climate event. *Geophys. Res. Lett.* 34 <https://doi.org/10.1029/2007GL031318>.
- Culver, S.J., 1988. New Foraminiferal Depth Zonation of the Northwestern Gulf of Mexico. *PALAIOS* 3, 69–85. <https://doi.org/10.2307/3514545>.
- Culver, S.J., Woo, H.J., Oertel, G.F., Buzas, M.A., 1996. Foraminifera of coastal depositional environments, Virginia, U.S.A.: distribution and taphonomy. *PALAIOS* 11, 459–486. <https://doi.org/10.2307/3515213>.
- Davis, R.A., Hayes, M.O., 1984. What is a Wave-Dominated Coast? In: Greenwood, B., Davis, R.A. (Eds.), *Developments in Sedimentology, Hydrodynamics and Sedimentation in Wave-Dominated Coastal Environments*. Elsevier, pp. 313–329. [https://doi.org/10.1016/S0070-4571\(08\)70152-3](https://doi.org/10.1016/S0070-4571(08)70152-3).
- FitzGerald, D.M., Fenster, M.S., Argow, B.A., Buynevich, I.V., 2008. Coastal Impacts due to Sea-level rise. *Annu. Rev. Earth Planet. Sci.* 36, 601–647. <https://doi.org/10.1146/annurev.earth.35.031306.140139>.
- Forcino, F.L., Leighton, L.R., Twerdy, P., Cahill, J.F., 2015. Reexamining Sample size Requirements for Multivariate, Abundance-based Community Research: when Resources are Limited, the Research does not have to be. *PLoS One* 10, e0128379. <https://doi.org/10.1371/journal.pone.0128379>.
- Garrett, E., Brain, M.J., Hayward, B.W., Newnham, R., Morey, C.J., Gehrels, W.R., 2023. Resolving uncertainties in foraminifera-based relative sea level reconstruction: a case study from southern New Zealand. *J. Foraminifera*. 53 (1), 78–89.
- Gehrels, W.R., 2013. *Microfossil-Based Reconstruction of Holocene Relative Sea Level Change*. Sea Level Studies.
- Goff, J.A., Allison, M.A., Gulick, S.P.S., 2010. Offshore transport of sediment during cyclonic storms: Hurricane Ike (2008), Texas Gulf Coast, USA. *Geology* 38, 351–354. <https://doi.org/10.1130/G30632.1>.
- Haslett, J., Parnell, A., 2008. A simple monotone process with application to radiocarbon-dated depth chronologies. *J. R. Stat. Soc.: Ser. C: Appl. Stat.* 57, 399–418. <https://doi.org/10.1111/j.1467-9876.2008.00623.x>.
- Hawkes, A.D., Horton, B.P., 2012. Sedimentary record of storm deposits from Hurricane Ike, Galveston and San Luis Islands, Texas. *Geomorphology* 171–172, 180–189. <https://doi.org/10.1016/j.geomorph.2012.05.017>.
- Heaton, T.J., Köhler, P., Butzin, M., Bard, E., Reimer, R.W., Austin, W.E.N., Ramsey, C.B., Grootes, P.M., Hughen, K.A., Kromer, B., Reimer, P.J., Adkins, J., Burke, A., Cook, M. S., Olsen, J., Skinner, L.C., 2020. Marine20—the Marine Radiocarbon Age Calibration Curve (0–55,000 cal BP). *Radiocarbon* 62, 779–820. <https://doi.org/10.1017/RDC.2020.68>.
- Jennings, A., Andrews, J., Pearce, C., Wilson, L., Ólafsdóttir, S., 2015. Detrital carbonate peaks on the Labrador shelf, a 13–7ka template for freshwater forcing from the Hudson Strait outlet of the Laurentide Ice Sheet into the subpolar gyre. *Quat. Sci. Rev.* 107, 62–80. <https://doi.org/10.1016/j.quascirev.2014.10.022>.
- Lambeck, K., Rouby, H., Purcell, A., Sun, Y., Sambdring, M., 2014. Sea level and global ice volumes from the last Glacial Maximum to the Holocene. *PNAS* 111, 15296–15303. <https://doi.org/10.1073/pnas.1411762111>.
- Leckie, R.M., Olson, H.C., 2003. Foraminifera as Proxies for Sea Level Change on Siliciclastic Margins.
- Maddox, J., Anderson, J.B., Milliken, K.T., Rodriguez, A.B., Dellapenna, T.M., Giosan, L., 2008. The Holocene evolution of the Matagorda and Lavaca estuary complex, Texas, USA. In: Anderson, J.B., Rodriguez, A.B. (Eds.), *Response of Upper Gulf Coast Estuaries to Holocene Climate Change and Sea-Level Rise*. *Geological Society of America*. [https://doi.org/10.1130/2008.2443\(07\)](https://doi.org/10.1130/2008.2443(07)), p. 0.
- Milliken, K.T., Anderson, J.B., Rodriguez, A.B., 2008. A new composite Holocene sea level curve for the northern Gulf of Mexico. In: *Response of Upper Gulf Coast Estuaries to Holocene Climate Change and Sea-Level Rise*, 443. *Geological Society of America Special Paper*, pp. 1–11.

- Milliken, K.T., Anderson, J.B., Rodriguez, A.B., 2008b. Record of dramatic Holocene environmental changes linked to eustasy and climate change in Calcasieu Lake, Louisiana, USA. In: Anderson, J.B., Rodriguez, A.B. (Eds.), Response of Upper Gulf Coast Estuaries to Holocene Climate Change and Sea-Level Rise. Geological Society of America. [https://doi.org/10.1130/2008.2443\(04\)](https://doi.org/10.1130/2008.2443(04)), p. 0.
- Milliken, K.T., Anderson, J.B., Rodriguez, A.B., 2008c. Tracking the Holocene evolution of Sabine Lake through the interplay of eustasy, antecedent topography, and sediment supply variations, Texas and Louisiana, USA. In: Anderson, J.B., Rodriguez, A.B. (Eds.), Response of Upper Gulf Coast Estuaries to Holocene Climate Change and Sea-Level Rise. Geological Society of America. [https://doi.org/10.1130/2008.2443\(05\)](https://doi.org/10.1130/2008.2443(05)), p. 0.
- NOAA, 2023. Sea Level Trends, National Ocean and Atmospheric Administration. <https://tidesandcurrents.noaa.gov/sltrends/>.
- NOAA National Centers for Environmental Information, 2023. Coastal Relief Models (CRMs) [Data set]. NOAA National Centers for Environmental Information. <https://doi.org/10.25921/5ZNS-KN44>.
- Nordt, L.C., Boutton, T.W., Hallmark, C.T., Waters, M.R., 1994. Late Quaternary Vegetation and climate changes in Central Texas based on the Isotopic Composition of Organic Carbon. *Quat. Res.* 41, 109–120.
- Nordt, L.C., Boutton, T.W., Jacob, J.S., Mandel, R.D., 2002. C4 Plant Productivity and Climate-CO2 Variations in South-Central Texas during the late Quaternary. *Quat. Res.* 58, 182–188. <https://doi.org/10.1006/qres.2002.2344>.
- Olson, H.C., Leckie, R.M. (Eds.), 2003. Micropaleontologic Proxies for Sea Level Change and Stratigraphic Discontinuities. SEPM (Society for Sedimentary Geology). <https://doi.org/10.2110/pec.03.75>.
- Palermo, R.V., Piliouras, A., Swanson, T.E., Ashton, A.D., Mohrig, D., 2021. The effects of storms and a transient sandy veneer on the interannual planform evolution a low-relief coastal cliff and wave-cut platform at Sargent Beach, Texas, USA. *Earth Surf. Dynam. Discuss.* 1–20.
- Phleger, F.B., 1951. Ecology of Foraminifera, Northwest Gulf of Mexico. Geological Society of America.
- Phleger, F.B., 1960. Sedimentary patterns of Microfaunas in Northern Gulf of Mexico. In: Shepard, F.P., Phleger, F.B., Andel, T.H.V. (Eds.), Recent Sediments, Northwest Gulf of Mexico. American Association of Petroleum Geologists. <https://doi.org/10.1306/SV21353C10>, p. 0.
- Phleger, F.B., 1965. Patterns of Marsh Foraminifera, Galveston Bay, Texas. *Limnol. Oceanogr.* 10, R169–R184. <https://doi.org/10.4319/lo.1965.10.suppl2.r169>.
- Poag, C.W., 1981. Benthic Foraminifera of the Gulf of Mexico.
- Poag, C.W., 2015. Benthic Foraminifera of the Gulf of Mexico: Distribution, Ecology, Paleogeology. Texas A&M University Press.
- Ramsey, C.B., 2009. Bayesian Analysis of Radiocarbon Dates. *Radiocarbon* 51, 337–360. <https://doi.org/10.1017/S0033822200033865>.
- Rehker, L.J., 1969. Sedimentology of Holocene Estuarine Deposits. *Galvest. Bay* 12–52.
- Reimer, P.J., Austin, W.E.N., Bard, E., Bayliss, A., Blackwell, P.G., Ramsey, C.B., Butzin, M., Cheng, H., Edwards, R.L., Friedrich, M., Grootes, P.M., Guilderson, T.P., Hajdas, I., Heaton, T.J., Hogg, A.G., Hughen, K.A., Kromer, B., Manning, S.W., Muscheler, R., Palmer, J.G., Pearson, C., van der Plicht, J., Reimer, R.W., Richards, D.A., Scott, E.M., Southon, J.R., Turney, C.S.M., Wacker, L., Adolphi, F., Büntgen, U., Capano, M., Fahrni, S.M., Fogtmann-Schulz, A., Friedrich, R., Köhler, P., Kudsk, S., Miyake, F., Olsen, J., Reinig, F., Sakamoto, M., Sookdeo, A., Talamo, S., 2020. The IntCal20 Northern Hemisphere Radiocarbon Age Calibration Curve (0–55 cal kBP). *Radiocarbon* 62, 725–757. <https://doi.org/10.1017/RDC.2020.41>.
- Rodriguez, A.B., 1999. Sedimentary Facies and Evolution of Late Pleistocene to Recent Coastal Lithosomes on the East Texas Shelf (Thesis).
- Rodriguez, A.B., Anderson, J.B., Siringan, F.P., Taviani, M., 1999. Sedimentary Facies and Genesis of Holocene Sand Banks on the East Texas Inner Continental Shelf. <https://doi.org/10.2110/pec.99.64.0165>.
- Rodriguez, A.B., Fassell, M.L., Anderson, J.B., 2001. Variations in shoreface progradation and ravinement along the Texas coast, Gulf of Mexico. *Sedimentology* 48, 837–853. <https://doi.org/10.1046/j.1365-3091.2001.00390.x>.
- Rodriguez, A.B., Anderson, J.B., Siringan, F.P., Taviani, M., 2004. Holocene Evolution of the East Texas Coast and Inner Continental Shelf: Along-strike Variability in Coastal Retreat Rates. *J. Sediment. Res.* 74, 405–421. <https://doi.org/10.1306/092403740405>.
- Rodriguez, A.B., Anderson, J.B., Simms, A.R., 2005. Terrace Inundation as an Autocyclic Mechanism for Parasequence Formation: Galveston Estuary, Texas, U.S.A. *J. Sediment. Res.* 75, 608–620. <https://doi.org/10.2110/jsr.2005.050>.
- Rodriguez, A.B., Duran, D.M., Mattheus, C.R., Anderson, J.B., 2008a. Sediment accommodation control on estuarine evolution: an example from Weeks Bay, Alabama, USA. In: Anderson, J.B., Rodriguez, A.B. (Eds.), Response of Upper Gulf Coast Estuaries to Holocene Climate Change and Sea-Level Rise. Geological Society of America. [https://doi.org/10.1130/2008.2443\(03\)](https://doi.org/10.1130/2008.2443(03)), p. 0.
- Rodriguez, A.B., Greene Jr., D.L., Anderson, J.B., Simms, A.R., 2008b. Response of Mobile Bay and eastern Mississippi Sound, Alabama, to changes in sediment accommodation and accumulation. In: Anderson, J.B., Rodriguez, A.B. (Eds.), Response of Upper Gulf Coast Estuaries to Holocene Climate Change and Sea-Level Rise. Geological Society of America. [https://doi.org/10.1130/2008.2443\(02\)](https://doi.org/10.1130/2008.2443(02)), p. 0.
- Shawler, J.L., Ciarletta, D.J., Connell, J.E., Boggs, B.Q., Lorenzo-Trueba, J., Hein, C.J., 2021. Relative influence of antecedent topography and sea-level rise on barrier-island migration. *Sedimentology* 68, 639–669. <https://doi.org/10.1111/sed.12798>.
- Simms, A.R., Anderson, J.B., Rodriguez, A.B., Taviani, M., 2008. Mechanisms controlling environmental change within an estuary: Corpus Christi Bay, Texas, USA. In: Anderson, J.B., Rodriguez, A.B. (Eds.), Response of Upper Gulf Coast Estuaries to Holocene Climate Change and Sea-Level Rise. Geological Society of America. [https://doi.org/10.1130/2008.2443\(08\)](https://doi.org/10.1130/2008.2443(08)), p. 0.
- Simms, A.R., Aryal, N., Miller, L., Yokoyama, Y., 2010. The incised valley of Baffin Bay, Texas: a tale of two climates. *Sedimentology* 57, 642–669. <https://doi.org/10.1111/j.1365-3091.2009.01111.x>.
- Siringan, F.P., 1993. Coastal Lithosome Evolution and Preservation during an Overall Rising Sea Level: East Texas Gulf Coast and Continental Shelf (Thesis).
- Siringan, F.P., Anderson, J.B., 1993. Seismic facies, architecture, and evolution of the Bolivar roads tidal inlet/delta complex, East Texas Gulf Coast. *J. Sediment. Res.* 63, 794–808. <https://doi.org/10.1306/D4267C08-2B26-11D7-8648000102C1865D>.
- Siringan, F.P., Anderson, J.B., 1994. Modern shoreface and inner-shelf storm deposits off the East Texas Coast, Gulf of Mexico. *J. Sediment. Res.* B64, 99–110.
- Swartz, J.M., 2019. Channel Processes and Products in Subaerial and Submarine Environments across the Gulf of Mexico. University of Texas, Austin, Tex.
- Swartz, J., Standing, P., Goff, J.A., Gulick, S., Lowery, C.M., 2022. Coastal River Response to Transgression: A New Look at the Trinity Incised Valley Using Multi-Resolution Seismic Imaging.
- Thomas, M.A., Anderson, J.B., 1994. Sea Level Controls on the Facies Architecture of the Trinity/Sabine Incised-Valley System. *Texas Continental Shelf*.
- Törnqvist, T.E., Bick, S.J., González, J.L., van der Borg, K., de Jong, A.F.M., 2004. Tracking the sea level signature of the 8.2 ka cooling event: New constraints from the Mississippi Delta. *Geophys. Res. Lett.* 31 <https://doi.org/10.1029/2004GL021429>.
- Troiani, B.T., Simms, A.R., Dellapenna, T., Piper, E., Yokoyama, Y., 2011. The importance of sea level and climate change, including changing wind energy, on the evolution of a coastal estuary: Copano Bay, Texas. *Mar. Geol.* 280, 1–19.
- Ullman, D.J., Carlson, A.E., Hostetler, S.W., Clark, P.U., Cuzzone, J., Milne, G.A., Winsor, K., Caffee, M., 2016. Final Laurentide ice-sheet deglaciation and Holocene climate-sea level change. *Quat. Sci. Rev.* 152, 49–59. <https://doi.org/10.1016/j.quascirev.2016.09.014>.
- Vitousek, S., Barnard, P.L., Fletcher, C.H., Frazer, N., Erikson, L., Storlazzi, C.D., 2017. Doubling of coastal flooding frequency within decades due to sea-level rise. *Sci. Rep.* 7, 1399. <https://doi.org/10.1038/s41598-017-01362-7>.
- Wagner, A.J., Guilderson, T.P., Slowey, N.C., Cole, J.E., 2009. Pre-Bomb Surface Water Radiocarbon of the Gulf of Mexico and Caribbean as Recorded in Hermatypic Corals. *Radiocarbon* 51, 947–954. <https://doi.org/10.1017/S0033822200034020>.
- Wantland, K.F., 1969. Distribution of Modern Brackish-Water Foraminifera in Trinity Bay 93–117.
- Weight, R.W.R., Anderson, J.B., Fernandez, R., 2011. Rapid Mud Accumulation on the Central Texas Shelf Linked to climate change and Sea-level rise. *J. Sediment. Res.* 81, 743–764. <https://doi.org/10.2110/jsr.2011.57>.
- Wellner, J.S., Sarzalejo, S., Lagoe, M., Anderson, J.B., 2004. Late quaternary stratigraphic evolution of the West Louisiana/East Texas Continental Shelf. In: Anderson, J.B., Fillon, R.H. (Eds.), Late Quaternary Stratigraphic Evolution of the Northern Gulf of Mexico Margin. SEPM Society for Sedimentary Geology. <https://doi.org/10.2110/pec.04.79.0217>, p. 0.
- Williams, H.F.L., 1994. Intertidal Benthic Foraminiferal Biofacies on the Central Gulf Coast of Texas: Modern distribution and Application to Sea Level Reconstruction. *Micropaleontology* 40, 169–183. <https://doi.org/10.2307/1485774>.
- Woo, H.J., Culver, S.J., Oertel, G.F., 1997. Benthic Foraminiferal Communities of a Barrier-Lagoon System, Virginia, U.S.A. *J. Coast. Res.* 13, 1192–1200.

## Further-reading

- Toomey, R.S., Blum, M.D., Valastro, S., 1993. Late Quaternary climates and environments of the Edwards Plateau, Texas. *Glob. Planet. Chang.* 7, 299–320. [https://doi.org/10.1016/0921-8181\(93\)90003-7](https://doi.org/10.1016/0921-8181(93)90003-7).